Bioorganic Chemistry 115 (2021) 105181

Contents lists available at ScienceDirect

Bioorganic Chemistry

journal homepage: www.elsevier.com/locate/bioorg

N-(3-cyano-1*H*-indol-5-yl)isonicotinamide and *N*-(3-cyano-1*H*-indol-5-yl)-1*H*-benzo[*d*]imidazole-5-carboxamide derivatives: Novel amide-based xanthine oxidase inhibitors

Shun Tu [1], Ting-jian Zhang [1], Yi Zhang, Xu Zhang, Zhen-hao Zhang, Fan-hao Meng [*]

School of Pharmacy, China Medical University, 77 Puhe Road, North New Area, Shenyang 110122, China

ARTICLE INFO

Keywords:
Synthesis
Xanthine oxidase inhibitor
SAR
Hyperuricemia

ABSTRACT

Our previous work demonstrated that amide is an efficient linker to explore chemical space of xanthine oxidase (XO) inhibitors that are entirely different from febuxostat and topiroxostat. In this effort, with 3-cyano-1*H*-indol-5-yl as a key moiety, two series of amide-based XO inhibitors, *N*-(3-cyano-1*H*-indol-5-yl)isonicotinamides (**2a-w**) and *N*-(3-cyano-1*H*-indol-5-yl)-1*H*-benzo[*d*]imidazole-5-carboxamides (**3a-i**), were designed and synthesized. The structure-activity relationship investigation identified *N*-(3-cyano-1-cyclopentyl-1*H*-indol-5-yl)-1*H*-benzo[*d*]imidazole-5-carboxamide (**3i,** IC_{50} = 0.62 μM) as the most promising compound, with 14.4-fold higher *in vitro* inhibitory potency than allopurinol (IC_{50} = 8.91 μM). Molecular simulations provided reasonable interaction modes for the representative compounds. Furthermore, *in vivo* activity evaluation demonstrated that compound **3i** (oral dose of 12.8 mg/kg) has obviously hypouricemic effect on a potassium oxonate induced hyperuricemic rat model. Cytotoxicity assay and ADME prediction also supported that **3i** is an excellent lead for further exploration of amide-based XO inhibitors.

1. Introduction

Hyperuricemia is a chronic metabolic disease with elevated serum uric acid caused by purine metabolism disorder [1,2]. Serum uric acid is the final oxidation product of human purine catabolism, and the continuous increase of serum uric acid will induce the formation of monosodium urate crystal deposits, eventually leading to gout [3]. Besides, high levels of serum uric acid are associated with many other chronic diseases, such as cardiovascular disease, hypertension, and kidney disease [4–6]. Xanthine oxidase (XO) is a multifunctional molybdoflavin protein and a key rate-limiting enzyme in the purine metabolic pathway [7]. XO can catalyze the oxidation of hypoxanthine and xanthine to uric acid and generate reactive oxygen species (ROS) [8,9]. Excessive ROS can cause cell damage and participate in many pathological processes, such as diabetes, atherosclerosis, and chronic heart failure [10]. Therefore, XO has become an important target, not only for the treatment of gout and hyperuricemia but also for many other diseases related to ROS [9,11].

Allopurinol is a hypoxanthine isomer that has been used to treat hyperuricemia and gout for decades [12]. However, as purine analog, allopurinol and other purine-type XO inhibitors affect purine metabolism and cause serious side effects, including fever, liver damage, kidney damage, and Stevens-Johnson syndrome [13]. In the past ten years, many nonpurine-based XO inhibitors with different scaffolds have been released, including furans [14] pyrano[3,2-*d*]pyrimidines [15] flavonoids [16,17] imidazoles [18] 5-aryl-1*H*-tetrazoles [19] thiazole-5-carboxylic acid derivatives [20] dihydropyrimidine-5-carboxylic acid derivatives [21] 5-arylazo-tropolone derivatives [22] caffeic acid phenethyl ester derivatives [23] and chalcone derivatives [24,25]. In clinical application, nonpurine XO inhibitor febuxostat was approved by the US Food and Drug Administration (FDA) in 2009, and another nonpurine XO inhibitor, topiroxostat, was subsequently approved by the Japanese Food and Drug Administration in 2013. Both topiroxostat and febuxostat are novel nonpurine XO inhibitors based on the characteristic five-membered ring linker. However, after clinical application, it was found that topiroxostat may increase the incidence of gouty arthritis [26]. And on February 21, 2019, FDA added a boxed warning for increased risk for heart-related death with febuxostat. Hence, novel nonpurine XO inhibitors are still urgently needed to meet the clinical requirement.

* Corresponding author.
E-mail address: fhmeng@cmu.edu.cn (F.-h. Meng).
[1] These two authors contributed equally to this work.

https://doi.org/10.1016/j.bioorg.2021.105181
Received 30 November 2020; Received in revised form 5 July 2021; Accepted 12 July 2021
Available online 15 July 2021

In recent years, our team has been engaged in the discovery of novel XO inhibitors, and numerous promising compounds with diverse chemotypes have been published [9,27–33]. Especially, through employing amide fragment to be an opened-ring isostere of five-membered ring linker of classic XO inhibitors (*e.g.*, thiazole of febuxostat and 1,2,4-triazole of topiroxostat), we successfully identified *N*-phenylisonicotinamide, as a novel XO inhibitor scaffold for the first time [27]. This finding provides important clues for the discovery of novel XO inhibitors bearing an amide linker (amide-based XO inhibitors). In the present work, amide-based XO inhibitors with stronger structural diversity were further explored.

Guiding by the structure based drug design (CBDD), we speculated that introducing larger aromatic (such as fused aromatic ring) on one or both sides of the amide linker may balance two vital H-bond interactions with residues Asn768 and Glu1261, respectively, and facilitate the binding affinity and inhibitory potency. Indole, as an endogenous biologically active substance and a popular drug construction fragment, has been widely used in the design of anti-tumor, anti-viral, anti-inflammatory, and even anti-hyperuricemia drugs [34–38]. Therefore, using indole as a key moiety, a series of *N*-(3-cyano-1*H*-indol-5-yl)isonicotinamide derivatives (**2a-w**) was firstly designed and synthesized. Furthermore, isonicotinamide, as the first discovered amide framework, despite exhibiting a great contribution to binding affinity (*e.g.*, forming π-π stack with Phe914 and generating hydrogen bonds with Glu1261), was assumed that it is not irreplaceable. Next, we utilized a bicyclic 5-1*H*-benzo[*d*]imidazole-5-carbonyl moiety to replace the monocyclic isonicotinoyl moiety of **2a-w** to provide another series of XO inhibitors, *N*-(1*H*-indol-5-yl)-1*H*-benzo[*d*]imidazole-5-carboxamide derivatives (**3a-i**) as shown in Fig. 1. Additionally, 3′-cyano was introduced onto the indole moiety to serve as an H-bond receptor to interact with Asn768 residue of XO, and the substituent linked at 1′-position was expected to form hydrophobic interaction with lipophilic amino acid residues(such as Leu648, Phe649, and Phe1013).

After the structure-activity relationship investigations, the most potent compounds were submitted to steady-state kinetic analysis and molecular simulations studies to investigate the inhibition behaviors. Meanwhile, the *in vivo* hypouricemic effects, cytotoxicity and ADMET (absorption, distribution, metabolism, excretion, and toxicity) prediction were further performed for the optimized compound.

2. Results and discussion

2.1. Chemistry

The synthesis of *N*-(1-alkyl-3-cyano-1H-indol-5-yl) isonicotinamides (**2a-i**), *N*-(1-alkyl-3-cyano-1H-indol-5-yl)-2-chloroisonicotinamides (**2j-o**) and *N*-(1-alkyl-3-cyano-1H-indol-5-yl)-2-fluoroisonicotinamides (**2p-w**) was performed as outlined in Scheme 1. The formyl group was introduced into commercially available 5-nitro-1*H*-indole under Vilsmeier-Haack conditions to provide 5-nitro-1*H*-indole-3-carbaldehyde (**4**) [40]. The corresponding formyl group was further converted into a cyano group in the presence of hydroxylamine hydrochloride and sodium formate in formic acid at reflux to afford 5-nitro-1*H*-indole-3-carbonitriles (**5**) [41]. The reduction of **5** by hydrogen under the catalysis of Pd/C yielded 5-amino-1*H*-indole-3-carbonitrile (**6**), which was acylated with corresponding acyl chloride in the presence of triethylamine to provide *N*-(1-alkyl-3-cyano-1H-indol-5-yl) heterocyclic amides (**2a**, **2j**, **2o,** and **3a**) [42,43]. Alkylation of compounds (**2a**, **2j**, and **2o**) with various alkyl chlorides or alkyl bromides obtained *N*-(1-alkyl-3-cyano-1H-indol-5-yl) heterocyclic amides (**2a-w**) [44].

The synthesis of *N*-(1-alkyl-3-cyano-1*H*-indol-5-yl)-1*H*-benzo[*d*]imidazole-6-carboxamide (**3b-i**) was carried out by a similar procedure as shown in Scheme 2. 5-nitro-1*H*-indole-3-carbonitrile (**5**) was alkylated with various alkyl chlorides or alkyl bromides in the presence of sodium hydride in dimethylformamide (DMF) to give 1- alkyl-5-nitro-1*H*-indole-3-carbonitrile (**7**). The reduction of **7** by tin chloride dehydrate in the presence of hydrochloric acid yielded 1-alkyl-5-amino-1*H*-indole-3-carbonitrile (**8**), which was acylated with 1*H*-benzo[*d*]imidazole-6-carbonyl chloride in the presence of triethylamine to provide *N*-(1-alkyl-3-cyano-1*H*-indol-5-yl)-1*H*-benzo[*d*]imidazole-6-carboxamide (**3b-i**) [45].

The synthesis of *N*-(1*H*-indol-5-yl)isonicotinamide (**10**) and N-(3-formyl-1*H*-indol-5-yl)isonicotinamide (**11**) were carried out by a similar procedure as shown in Scheme 3. Commercially available 5-nitroindole was reduced by hydrogen under the catalysis of Pd/C to yield 1*H*-indol-5-amine (**9**), which was acylated with isonicotinoyl chloride in the presence of triethylamine to provide *N*-(1*H*-indol-5-yl)isonicotinamide (**10**). The formyl group was introduced into compound **10** under Vilsmeier-Haack conditions to provide *N*-(3-formyl-1*H*-indol-5-yl)isonicotinamide (**11**).

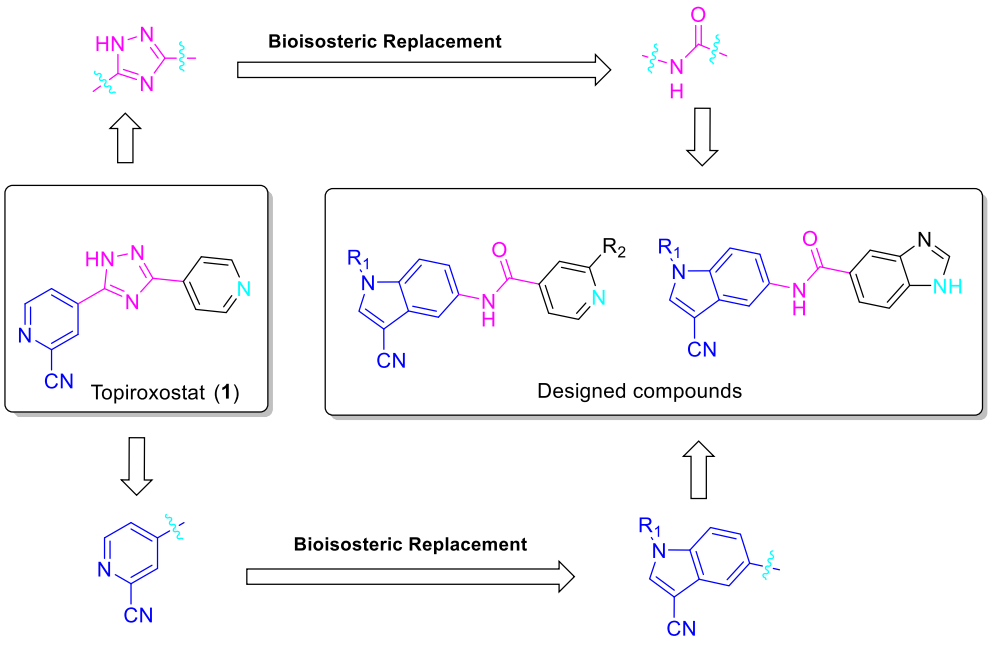

Fig. 1. Design strategy of the target compounds.

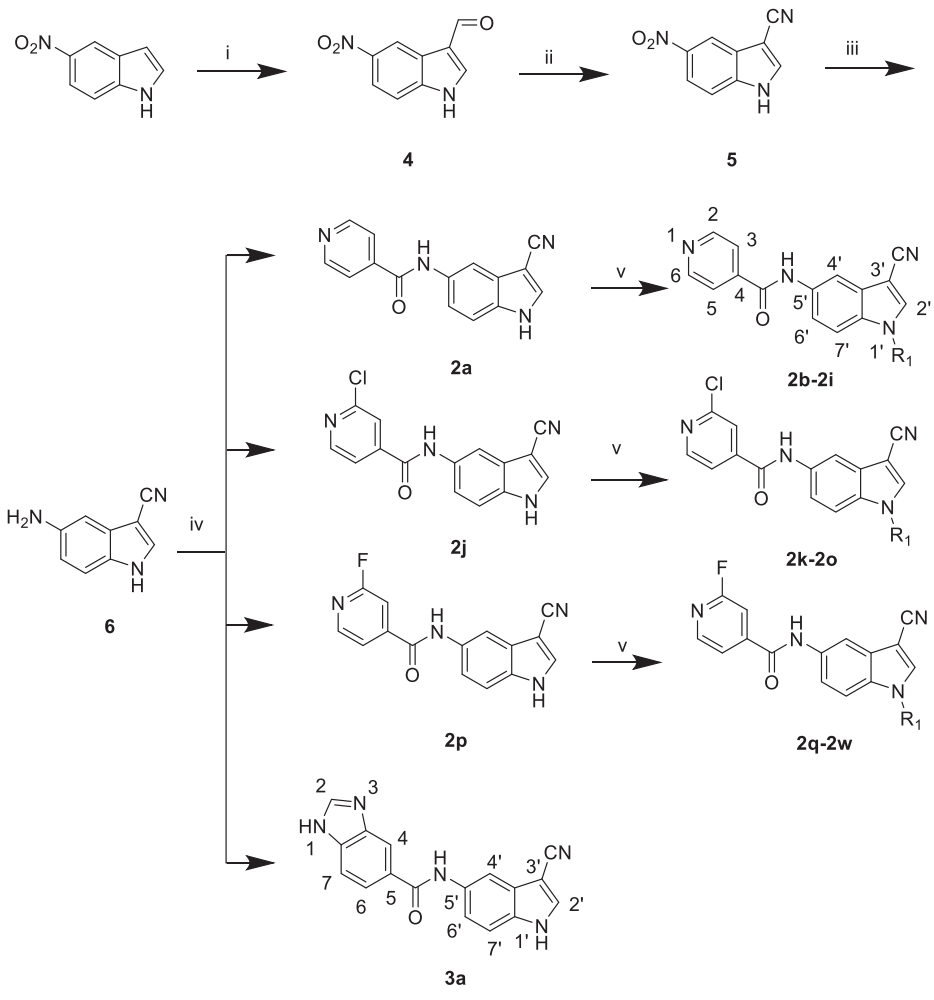

2b, R_1=methyl
2c, R_1=ethyl
2d, R_1= propyl
2e, R_1= *iso*-propyl
2f, R_1= allyl
2g, R_1= prop-2-yn-1-yl
2h, R_1= benzyl
2i, R_1= cyclopentyl
2k, R_1=methyl
2l, R_1=ethyl
2m, R_1= propyl
2n, R_1= *iso*-propyl
2o, R_1= allyl
2q, R_1=ethyl
2r, R_1= propyl
2s, R_1= *iso*-propyl
2t, R_1= allyl
2u, R_1= prop-2-yn-1-yl
2v, R_1= benzyl
2w, R_1= cyclopentyl

Scheme 1. Reagents and conditions: (i) $POCl_3$, DMF, 0 °C, 30 min, then room temperature overnight; (ii) $HONH_2HCl$, HCOONa, AcOH, 110 °C for 2 h; (iii) Pd/C, H_2, EtOH, 25 °C, 4 h; (iv) heterocyclic acid chloride, Et_3N, THF, −5 °C, 1 h, then room temperature overnight; (v) RCl or RBr, NaH, KI, DMF, −5 °C, 30 min, then 60 °C, overnight.

2.2. Biological activity in vitro

The *in vitro* bovine XO inhibitory activity of compounds **2a-t**, **3a-h**, **7a-d**, **11,** and **12** was measured spectrophotometrically by determining uric acid production at 294 nm. Topiroxostat and allopurinol were included as reference compounds. The testing results are shown in Table 1.

As shown in Table 1, in the *N*-(1-alkyl-3-cyano-1*H*-indol-5-yl)isonicotinamides series, except compounds **2b** (R_1 = methyl, not active, < 60% inhibition at 33 μM) and **2h** (R_1 = benzyl, IC_{50} = 12.46 μM), other compounds with different alkyl groups at the 1′-position of indole scaffold presented much higher potency than unsubstituted compound **2a** (IC_{50} = 8.59 μM). This indicated that the alkyl groups at 1′-position of the indole scaffold played a crucial role for these compounds. From methyl to ethyl, the efficiency varied from inactive to active, while, from ethyl to propyl, there was no obvious discrepancy in potency. Considering the potential steric effect, the length of the alkyl at 1′-position of indole scaffold was initially locked within three carbon atoms. Therefore, the influence of some three atom carbon chains at 1′-position (**2d**, **2e**, **2f**, and **2 g**) was investigated. As indicated in Table 1, branched-chain alkyl groups may be more suitable for *N*-(1-alkyl-3-cyano-1*H*-indol-5-yl)isonicotinamide than their straight-chain isostere (**2e** vs **2d**; IC_{50} = 4.43 μM vs 7.34 μM). When the propyl group was changed into allyl or propargyl, the potency was maintained (**2f** vs **2d**; IC_{50} = 7.65 μM vs 7.34 μM) or 6.2 times improved (**2g** vs **2d**; IC_{50} = 1.18 μM vs 7.34 μM). This demonstrated that unsaturated alkyl may be more conducive to *N*-(3-cyan-1*H*-indol-5-yl)isonicotinamide derivatives. When the 1′-position was substituted by a benzyl, the potency was weakened, (**2h** vs **2a**; IC_{50} = 12.46 μM vs 8.59 μM), while the introduction of a cyclopentyl significantly improved the potency (**2i** vs **2a**; IC_{50} = 0.73 μM vs 8.59 μM), suggesting that for *N*-(3-cyan-1*H*-indol-5-yl)isonicotinamide, the introduction of benzyl group may not be desirable while the substitution

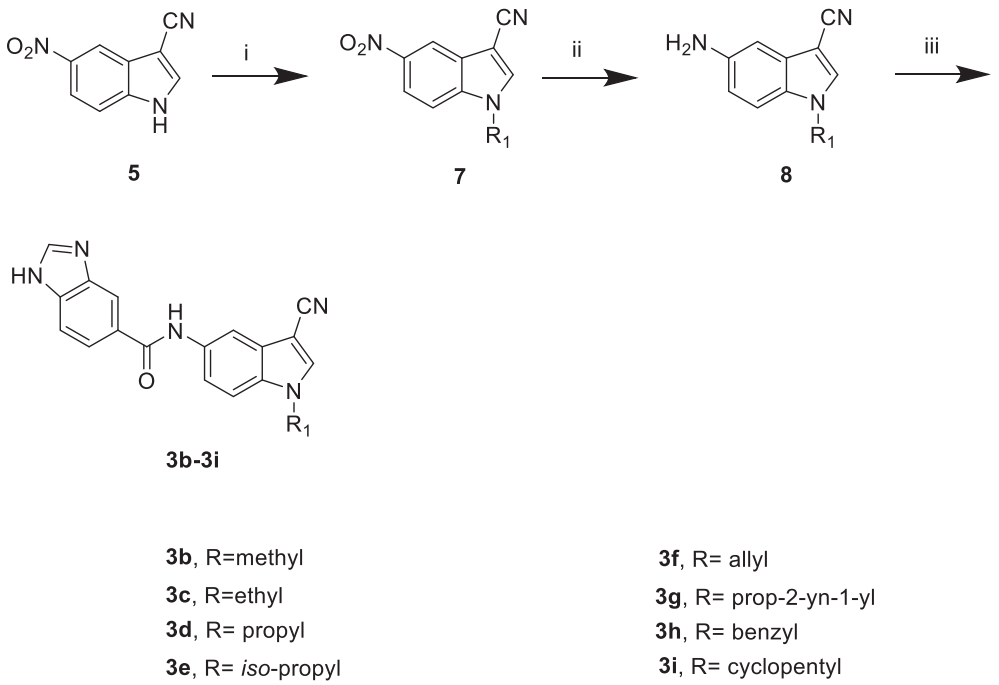

Scheme 2. Reagents and conditions: (i) RCl or RBr, NaH, KI, DMF, −5 °C, 30 min, then 60 °C, overnight; (ii) $SnCl_2$, HCl, EtOH, 60 °C, overnight; (iii) 1*H*-benzo[*d*] imidazole-5-carbonyl chloride, Et_3N, THF, −5 °C, 1 h, then room temperature overnight.

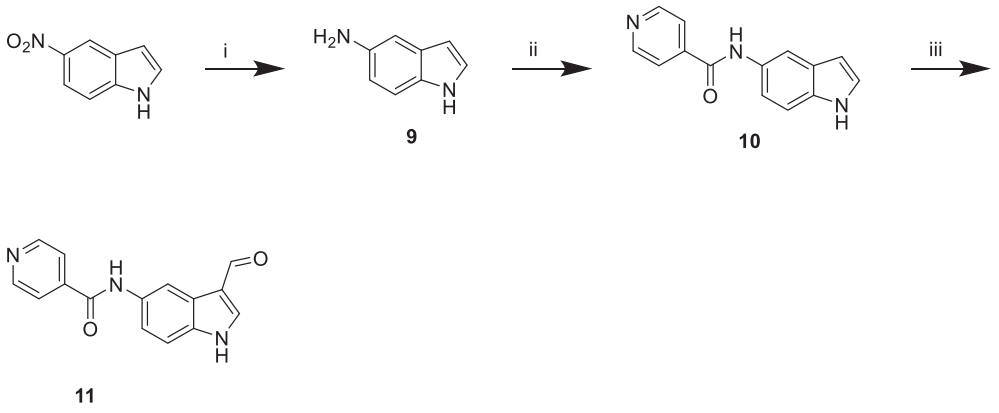

Scheme 3. Reagents and conditions: (i) Pd/C, H_2, EtOH, 25 °C, 18 h; (ii) isonicotinoyl chloride, Et_3N, THF, −5 °C, 1 h, then room temperature overnight; (iii) $POCl_3$, DMF, 0 °C, 30 min, then room temperature overnight.

of cyclopentyl would bring great benefits. Especially, cyclopentyl derivative **2i** displayed the highest inhibitory activity in the *N*-(1-alkyl-3-cyano-1*H*-indol-5-yl)isonicotinamides series, which was 12-fold better than compound **2a**. This result was also found in our previous studies [30]. In addition, when the 3′-position substitution of indole was changed into hydrogen (compound **11**, < 60% inhibition at 33 μM) or formyl group (compound **12**, < 60% inhibition at 33 μM), the potency disappeared, which indicated that maintaining the 3′-position cyano group was essential for potency.

To investigate the influence of halogen-substituted on isonicotinamide fragment, 2-chloro and 2-fluoro were introduced to provide *N*-(1-alkyl-3-cyano-1*H*-indol-5-yl)-2-chloroisonicotinamides and *N*-(1-alkyl-3-cyano-1*H*-indol-5-yl)-2-fluoroisonicotinamides. When chloro and fluoro were introduced at the 2-position of *N*-(1-alkyl-3-cyano-1H-indol-5-yl)isonicotinamide, the XO inhibitory activity was improvement (**2j** vs **2a**, and **2p** vs **2a** IC_{50} = 4.30 μM vs 8.59 μM, and IC_{50} = 6.95 μM vs 8.59 μM, respectively), which gave us considerable encouragement. Surprisingly, when alkyl groups were introduced at the 1′-position of the indole scaffold, the potency was not as generally improved as the isonicotinamide series, and even presented an opposite effect. Except for the slight increase in activity of compound **2u** (IC_{50} = 5.04 μM) relative to compound **2p**, the potency of other compounds reduced compared with compound **2j** or **2p**, some derivatives (*e.g.*, **2 k**, **2 l**, **2n**, **2o**, **2q**, **2 s,** and **2v**) even were inactive. And most of the derivatives with halogens introduced at the 2-position of isonicotinamide displayed weaker inhibitory potency than their corresponding counterparts in *N*-(1-alkyl-3-cyano-1*H*-indol-5-yl)isonicotinamides series (*e.g.*, **2 l** vs **2c**, **2q** vs **2c**, **2n** vs **2d**, **2 s** vs **2d**, and **2u** vs **2 g**), indicating that the introduction of halogens at the 2-position of isonicotinamide series were detrimental to the XO inhibitory activity.

Generally speaking, *N*-(1-alkyl-3-cyano-1*H*-indol-5-yl)-1*H*-benzo[*d*] imidazole-5-carboxamide exhibited higher XO inhibitory activity than *N*-(1-alkyl-3-cyano-1*H*-indol-5-yl)isonicotinamide counterpart (*e.g.*, **3a** vs **2a**, **3b** vs **2b**, **3c** vs **2c**, **3d** vs **2d**, **3f** vs **2f**, and **3h** vs **2h**), which revealed that the benzo[*d*]imidazole-5-carboxamide may be more effective than isonicotinamide moiety. And with the extension of the length of the alkyl groups at 1′-position (**3b**, **3c**, **3d** IC_{50} = 4.49 μM, 2.16 μM, 2.17 μM, respectively), the variation pattern of efficacy showed

Table 1

In vitro XO inhibitory potency of compounds.

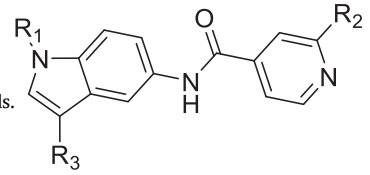

2a-2w, **10** and **11**

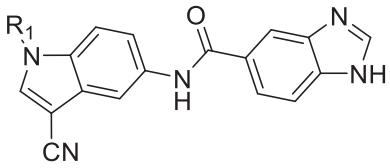

3a-3i

Compounds	R_1 groups	R_2 groups	R_3 groups	IC_{50}(μM)[a]
2a	H	H	CN	8.59 ± 0.19
2b	Methyl	H	CN	n.a.[b]
2c	Ethyl	H	CN	7.89 ± 0.16[c]
2d	Propyl	H	CN	7.34 ± 0.14[c]
2e	*iso*-Propyl	H	CN	4.43 ± 0.12
2f	Allyl	H	CN	7.65 ± 0.24[c]
2g	Prop-2-yn-1-yl	H	CN	1.18 ± 0.06[c]
2h	Benzyl	H	CN	12.46 ± 0.66
2i	Cyclopentyl	H	CN	0.73 ± 0.02
2j	H	Cl	CN	4.30 ± 0.24
2k	Methyl	Cl	CN	n.a.
2l	Ethyl	Cl	CN	n.a.
2m	Propyl	Cl	CN	16.19 ± 1.32
2n	*iso*-Propyl	Cl	CN	n.a.
2o	Allyl	Cl	CN	n.a.
2p	H	F	CN	6.95 ± 0.29[c]
2q	Ethyl	F	CN	n.a.
2r	Propyl	F	CN	12.64 ± 1.10
2s	*iso*-Propyl	F	CN	n.a.
2t	Allyl	F	CN	21.79 ± 1.21
2u	Prop-2-yn-1-yl	F	CN	5.04 ± 0.04[c]
2v	Benzyl	F	CN	n.a.
2w	Cyclopentyl	F	CN	12.64 ± 0.48
3a	H	/	/	3.52 ± 0.07
3b	Methyl	/	/	4.49 ± 0.13
3c	Ethyl	/	/	2.16 ± 0.22
3d	Propyl	/	/	2.17 ± 0.17
3e	*iso*-Propyl	/	/	4.25 ± 0.04
3f	Allyl	/	/	2.04 ± 0.07
3g	Prop-2-yn-1-yl	/	/	4.27 ± 0.34
3h	Benzyl	/	/	1.52 ± 0.03
3i	Cyclopentyl	/	/	0.62 ± 0.02[#]
10	H	H	H	n.a.
11	H	H	CHO	n.a.
Allopurinol	/	/	/	8.9 ± 0.09
Topiroxostat	/	/	/	0.021 ± 0.003

[a] Values are means ± SD of three independent experiments.
[b] n.a.: not active (<60% inhibition at 33 μM).
[c] $P < 0.05$, versus allopurinol.
[#] $P < 0.05$, versus compound **2i**.

similarity to that of *N*-(1-alkyl-3-cyano-1*H*-indol-5-yl)isonicotinamides series. Interestingly, the effect of alkyl groups at 1′-position with three carbon atom lengths on inhibitory potency differed from that of the *N*-(1-alkyl −3-cyano-1*H*-indol-5-yl)isonicotinamides series. Straight chain alkyl may be more suitable for *N*-(1-alkyl-3-cyano-1H-indol-5-yl)-1*H*-benzo[*d*]imidazole-5-carboxamide than branched alkyl (**3d** vs **3e**; IC_{50} = 2.17 μM vs 4.25 μM). When the propyl group was replaced by allyl or propargyl group, the potency was remained (**3f** vs **3d**; IC_{50} = 2.04 μM vs 2.17 μM) or decreased (**3g** vs **3d**; IC_{50} = 1.18 μM vs 4.27 μM), indicating that saturated alkyl may be more conducive to *N*-(3-cyan-1*H*-indol-5-yl)−1*H*-benzo[*d*]imidazole-5-carboxamide derivatives. The introduction of benzyl and cyclopentyl both improved the XO inhibitory activity (**3h** vs **3a**, and **3i** vs **3a** IC_{50} = 1.52 μM vs 3.52 μM, and IC_{50} = 0.62 μM vs 3.52 μM, respectively), especially compound **3i** presented as the most potent compound in this work. On the whole, the introduction of a small alkyl group at the 1′-position was advantageous to the XO inhibitory effect of *N*-(1-alkyl-3-cyano-1H-indol-5-yl)-1*H*-benzo[*d*]imidazole-5-carboxamide, which was similar to the *N*-(1-alkyl-3-cyano-1*H*-indol-5-yl)isonicotinamides series. Moreover, in these two series, compounds **2i** and **3i** with the best XO inhibitory activity both introduced cyclopentyl at the 1′-position. Compared with our previously discovered compound *N*-(3-cyano-4-(cyclopentyloxy)phenyl)isonicotinamide that possessed the same cyclopentyl substitution, the activities of compounds **2i** and **3i** have been greatly improved [27]. Particularly, compound **3i** exhibited 14.4-fold higher potency than the positive control allopurinol (IC_{50} = 8.9 μM), although, it still 30-fold less effective than another positive control topiroxostat (IC_{50} = 0.021 μM). To investigate the inhibition type of compound **3i** on XO, enzyme kinetics studies were performed. The Lineweaver-Burk plot (Fig. 2) revealed that compound **3i** acted as a mixed-type inhibitor. Additionally, the K_m and slope (K_m/V_{max}) were increased but the V_{max} was decreased by increasing the inhibitor concentration from 0 to 2.1 μM. Specifically, the K_m and V_{max} values of compound **3i** at 0 μM, 1 μM and 2.1 μM were 107.41, 253.56, and 387.00 μM and 43.69, 37.26, and 32.96 μM/min, respectively.

2.3. Molecular docking

To investigate the possible binding modes of these compounds in the XO catalytic pocket, the representative compounds, **2i** and **3i**, were subjected to molecular docking studies using MOE (Molecular Operating Environment, version 2015.1001, Chemical Computing Group Inc., Canada) software [46]. The crystal structure of XO in complex with

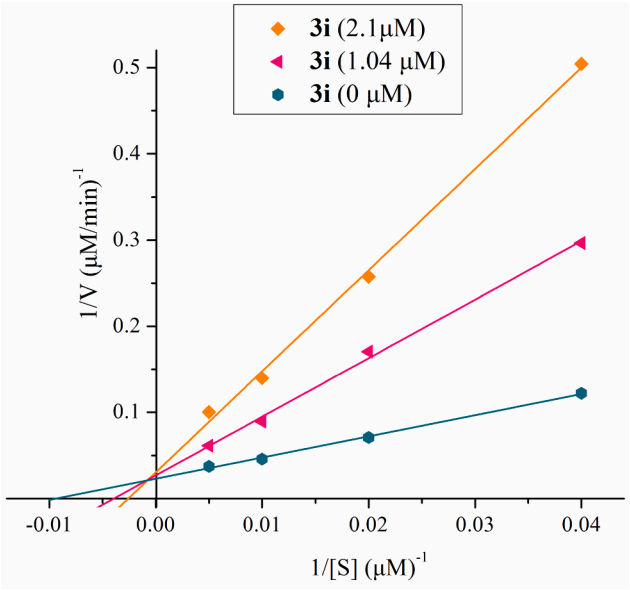

Fig. 2. Lineweaver-Burk plot analysis of XO inhibition by compound **3i**.

topiroxostat (PDB code: 1 V97) [39] was processed as a docking mode.

As shown in Fig. 3, two vital H-bond interactions were observed in both binding modes of **2i** (Fig. 3A) and **3i** (Fig. 3B), as expected, which were Asn768 residue forming H-bond with cyano group of both **2i** and **3i**, and Glu1261 interacting with pyridine N atom of **2i** and benzo[*d*] imidazole N atom of **3i**, respectively. This result verified our idea of balancing the interactions with residues Asn768 and Glu1261 by introducing an indole moiety. Moreover, amide fragments can strongly interact with amino acid residues Glu802 and Thr1010 in the active pocket as reported in our previous studies [39]. In addition, the cyclopentyl tail was surrounded by some lipophilic amino acid residues, such as Phe649, Leu648, and Phe1013, which may also contribute to the binding affinity. These interactions explained the relatively high activities of compounds **2i** and **3i**.

2.4. Molecular dynamics simulations

To obtain a more integrated and precise view of the binding process, molecular dynamics (MD) simulations of **3i** docking complex and topiroxostat/XO co-crystal (PDB code:1V97) were carried out using Groningen Machine for Chemicals Simulations (GROMACS) 5.0 package [47]. The backbone root means square deviation (RMSD) of the complex was exhibited in Fig. 4A. It can be seen from Fig. 4A that the RMSD values of the complexes XO/**3i** and XO/topiroxostat tended to be convergent with fluctuations around 2.3 Å and 2.3 Å respectively after 5 ns and 2 ns of simulation, clearly indicating that the whole system has been equilibrated. The balanced conformation was picked up and rendered with MOE software (Fig. 4B and 4C). As showed in Fig. 4C, after MD simulation, the conformational changes of topiroxostat in the active pocket were not significant, indicating that the MD protocol was reliable. And compound **3i** retained the majority of the interactions observed in molecular docking after MD simulation (Fig. 4B), such as the cyano group forming H-bond with Asn768, the benzo[*d*]imidazole N atom generating H-bond with Glu1261 residue, and the cyclopentyl tail interacting with lipophilic amino acid residues (*e.g.*, Phe649, Leu648, and Phe1013). Interestingly, the H-bond between amide NH and residue Glu802 disappeared; instead, the carbonyl accepted an H-bond from residue Thr1010.

2.5. Hypouricemic effect in vivo

The *in vivo* hypouricemic effects of compound **3i** were further investigated by measuring serum uric acid levels in an acute hyperuricemia rat model induced by potassium oxazinate. Topiroxostat was used as a positive control. Four experimental groups were set, which marked as blank group (normal rat orally administered blank solvent), model group (model rat orally administered blank solvent), **3i** group (model rat orally administered 12.8 mg/kg of **3i**) and topiroxostat group (model rat orally administered 10.0 mg/kg of topiroxostat), respectively. Oral doses of compound **3i** and topiroxostat had the same amount of substance. As shown in Fig. 5, compared with the blank group, the serum uric acid levels of the model group were markedly increased ($P < 0.01$), suggesting that the model was successfully established by intraperitoneal injection of potassium oxonate (300 mg/kg). Moreover, **3i** group showed an apparent reduction of 30.1% in uric acid levels ($P < 0.05$) at 2 h and a reduction of 20.8% in the AUC (uric acid, 0.5–8 h) ($P < 0.05$) compared with the model group. While topiroxostat group displayed a more obvious reduction of 73.9% in uric acid levels ($P < 0.0001$) at 2 h and a reduction of 66.4% in the AUC (uric acid, 0.5–8 h) ($P < 0.0001$) compared with the model group, which was 2.46 and 3.19 times more effective than compound **3i** in reducing serum uric acid levels, respectively. Thus, the results of the hypouricemic effect *in vivo* suggested that compound **3i** could be a promising lead compound for the treatment of hyperuricemia.

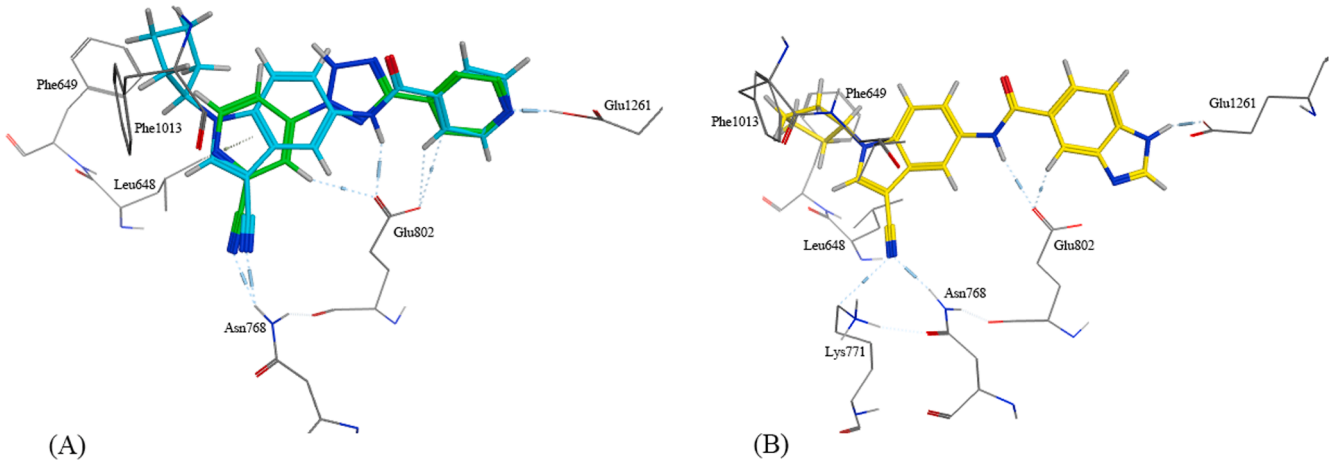

Fig. 3. Docking poses of compound **2i** (A, cyan) and **3i** (B, bright yellow) within the protein binding pocket and overlaid with the original ligand topiroxostat (green). (For interpretation of the references to colour in this figure legend, the reader is referred to the web version of this article.)

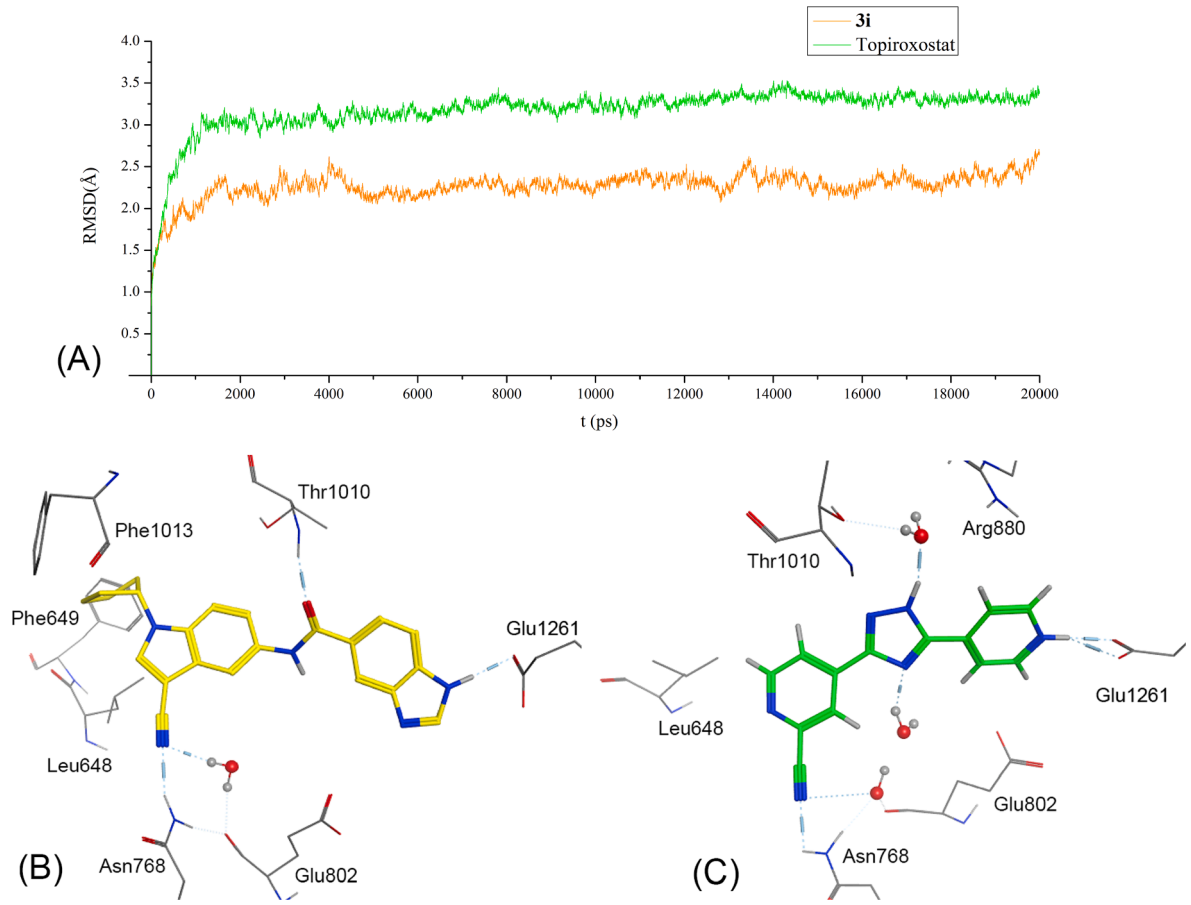

Fig. 4. Results of MD simulations. (A) Backbone RMSD of the complex versus time (20 ns); (B) MD conformation of XO in complex with compound **3i**; (C) MD conformation of XO in complex with topiroxostat.

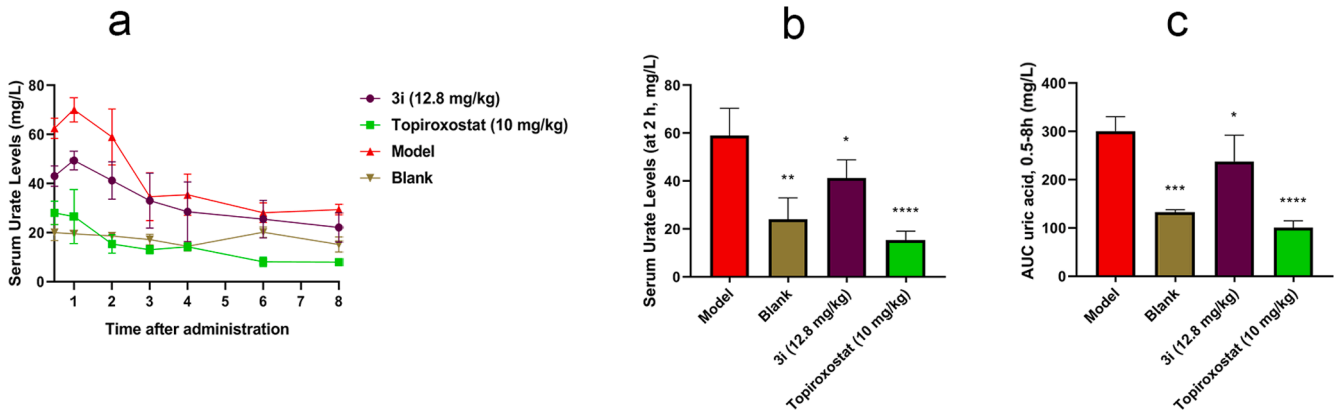

Fig. 5. Effect of compound **3i** and topiroxostat on the serum uric acid levels in the potassium oxonate-induced hyperuricemic rat model. (a) Time course changes of serum uric acid levels after 0.5–8 h of treatment. (b) Serum uric acid levels after 2 h of treatment. (c) The AUC of serum uric acid after 0.5–8 h of treatment. Blank group: normal rat orally administered blank solvent, model group: model rat orally administered blank solvent. The data are shown as the mean ± SD. (n = 6). *P < 0.05, **P < 0.01, ***P < 001 and ****P < 0.0001, significantly different from the model group by Student's *t*-test.

2.6. *In vitro cytotoxicity assay*

The MTT assay was used to evaluate the cytotoxicity of the compound **3i** in two healthy cell lines: MCF10A (human breast cells) and 16HBE (human bronchial epithelial cells). The cell viability assay data treated with different concentrations of **3i** (0.1 μM, 1 μM and 10 μM) were quantified (Fig. 6), and the highest incubation concentration was 16 times higher than IC_{50} value of **3i**. As shown in Fig. 6, MCF10A and 16HBE showed 91.06% and 81.14% cell viability at 10 μM, respectively, and both exhibited non-cytotoxicity on normal cells under the high concentration of 10 μM. It can be concluded that toxicity did not emerge from **3i** even after high-dose incubation.

2.7. *ADME/T properties prediction*

In order to assess the drug-like properties, pharmacokinetic behaviors (absorption, distribution, biotransformation and excretion) and toxicity of compound **3i** were predicted using pre-ADMET web service

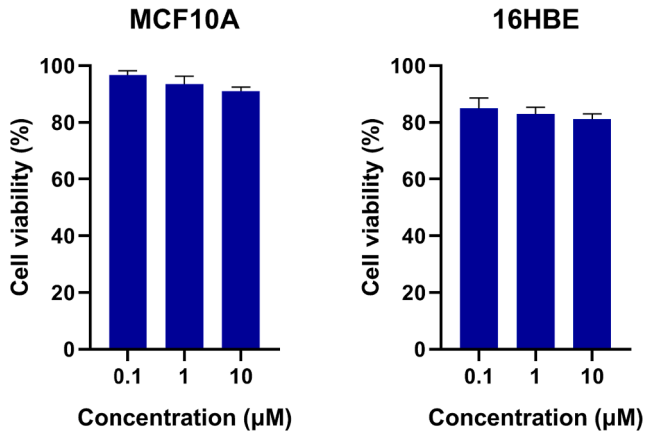

Fig. 6. Toxic effects of compound **3i** on healthy cell lines MCF10A and 16HBE.

(https://preadmet.bmdrc.kr/), and the results were summarized in Table 2 [48]. Low blood–brain barrier (BBB) permeability was found (C. brain/C.blood < 1), suggesting that **3i** could be inactive in the central nervous system. Importantly, Caco-2 permeability was used to evaluate the suitability of compounds for oral dosing, and **3i** has significantly better human intestinal permeability than allopurinol. In addition, human intestinal absorption (HIA) is a key factor that affects oral bioavailability, compound **3i** demonstrated excellent bioavailability. The high plasma-protein binding (PPB) of **3i** means a long half-life and stable efficacy, which could maintain a durable potency and adequate stability of the compound. The inhibition of CYP3A4 by a drug constitutes the majority of cases of drug-drug interaction; it was found that **3i** may not be an inhibitor of CYP3A4. Another hand, cardiotoxicity may not be avoided with the medium risk of hERG inhibition.

3. Conclusions

Herein, we designed and synthesized two series of amide-based XO inhibitors, *N*-(3-cyano-1*H*-indol-5-yl)isonicotinamides and *N*-(3-cyano-1*H*-indol-5-yl)-1*H*-benzo[*d*]imidazole-5-carboxamides. Biological evaluation indicated that the latter series are more active and more structurally diverse than the former series, indicating that amide is a versatile linker for designing novel XO inhibitor, and the chemical space of amide-based XO inhibitors is broad, and not limited in isonicotinamides. The structure-activity relationship investigation identified **3i** (IC_{50} = 0.62 μM) as the most potent compound, which exhibited 14.4-fold higher potency than the positive control allopurinol. During *in vivo* assay, compound **3i** showed an effective hypouricemic effect at an oral dose of 12.8 mg/kg in a rat model of potassium oxonate-induced hyperuricemia. MTT results indicated that compound **3i** is non-toxic to healthy cells at a high concentration of 10 μM. And ADME/T prediction supports the well drug-like properties of compound **3i.** In short, this work presented convincing evidence that *N*-(3-cyano-1*H*-indol-5-yl)-1*H*-benzo[*d*]imidazole-5-carboxamide could serve as a novel scaffold for the discovery and development of amide-based XO inhibitors, and compound **3i** could be a promising lead for the further investigation.

Table 2
Predicted ADMR/T profiles.[a]

ADME/Tox properties	Compound	
	3i	**Allopurinol**
Buffer solubility (SK atomic types, mg/L)	7.23	395.38
Blood-brain barrier penetration (BBB)	0.83	0.25
In vivo Caco-2 cell permeability (nm/sec)	20.17	16.61
Human intestinal absorption (HIA, %)	92.97	76.95
Plasma protein binding (PPB, %)	94.41	8.96
CYP_3A4_inhibition	Non	Inhibitor
CYP_3A4_substrate	Substrate	Weakly
hERG inhibition	Medium risk	Low risk

[a] https://preadmet.bmdrc.kr.

4. Experimental protocols

4.1. Chemistry

Unless otherwise indicated, reagents and solvents were purchased from commercial sources and used without further purification. All reactions were monitored by TLC using silica gel aluminum cards (0.2 mm thickness) with a fluorescent indicator of 254 nm. ^{1}H NMR and ^{13}C NMR spectra were recorded on a Bruker spectrometer. Chemical shifts were expressed in parts per million using tetramethylsilane as an internal reference and DMSO-d_6 as the solvent. ESI-HRMS data were gathered using a Bruker microTOF-Q instrument.

4.1.1. Synthesis of 5-nitro-1H-indole-3-carbaldehyde (4)

A mixture of anhydrous DMF (3.38 g, 46.25 mmol) and phosphorus oxychloride (14.18 g, 92.51 mmol) was stirred at 0 °C for 30 min. Then a solution of 5-nitro-1*H*-indole (5.00 g, 30.84 mmol) in anhydrous DMF (6 mL) was added dropwise to the above mixture. After the addition, the mixture was stirred at room temperature overnight. Then, the reaction mixture was poured into ice water, diluted with an aqueous solution of sodium hydroxide and refluxed for 1 h. After cooling, the precipitate was collected by filtration, washed with a large quantity of water and dried in vacuum to give 5-nitro-1*H*-indole-3-carbaldehyde **5** (5.34 g, yield 91.1%) as a brown solid. ^{1}H NMR (500 MHz, DMSO-d_6) δ 12.67 (s, 1H), 10.01 (s, 1H), 8.92 (s, 1H), 8.55 (s, 1H), 8.13 (d, J = 6.2 Hz, 1H), 7.70 (d, J = 6.6 Hz, 1H). ^{13}C NMR (125 MHz, DMSO-d_6) δ 185.34, 142.71, 141.24, 139.97, 123.36, 118.90, 118.61, 116.89, 113.06.

4.1.2. Synthesis of 5-nitro-1H-indole-3-carbonitrile (5)

A mixture of compound **4** (2.00 g, 10.52 mmol), hydroxylamine hydrochloride (3.65 g, 52.59 mmol) and sodium formate (3.93 g, 57.85 mmol) in formic acid (30 mL) was refluxed for 2 h. After that, the resulted solution was cooled and poured into ice water (400 mL). The formed precipitate was collected by filtration, washed with a large quantity of water and dried to provide 5-nitro-1*H*-indole-3-carbonitrile **5** (1.62 g, yield 82.2%) as a light yellow solid. ^{1}H NMR (500 MHz, DMSO-d_6) δ 12.81 (s, 1H), 8.53 (s, 1H), 8.49 (s, 1H), 8.14 (d, J = 8.8 Hz, 1H), 7.74 (d, J = 8.9 Hz, 1H). ^{13}C NMR (125 MHz, DMSO-d_6) δ 142.41, 138.31, 138.18, 125.86, 118.45, 114.91, 114.75, 113.65, 86.69.

4.1.3. Synthesis of 5-amino-1H-indole-3-carbonitrile (6)

A mixture of compound **5** (1.00 g, 5.34 mmol) and Pd/C (5%; 0.10 g) in ethanol (40 mL) under 40 psi of hydrogen atmosphere, was at 25 °C for 4 h. After the completion of the reaction, the insoluble solid was filtered out. The filtrate was evaporated under reduced pressure to give 5-amino-1*H*-indole-3-carbonitrile **6** (0.75 g, yield 89.4%) as an off-white solid. ^{1}H NMR (500 MHz, DMSO-d_6) δ 11.72 (s, 1H), 7.96 (d, J = 2.0 Hz, 1H), 7.22 (d, J = 8.6 Hz, 1H), 6.73 (s, 1H), 6.63 (d, J = 8.6 Hz, 1H), 4.92 (s, 2H). ^{13}C NMR (125 MHz, DMSO-d_6) δ 143.82, 132.73, 128.15, 128.13, 116.96, 113.42, 112.90, 100.44, 82.29.

4.1.4. General procedure for the synthesis of N-(1-alkyl-3-cyano-1H-indol-5-yl) heterocyclic amides (2a, 2j, 2p and 3a)

Into a solution of compound **6** (0.50 g, 3.18 mmol) and triethylamine (0.97 g, 9.54 mmol) in tetrahydrofuran (80 mL) at −5 °C, was added aroyl chloride (4.77 mmol). The mixture was maintained at the same temperature for 1 h and then stirred at room temperature overnight. After the completion of the reaction, the insoluble materials were removed by filtration and washed with THF. The filtrate was evaporated in vacuum to remove about 3/4 of the solvent. The residue was dispersed into water, filtered under reduced pressure, washed and dried to provide crude products, which was further purified by

recrystallization from 50% ethanol to provide corresponding products **2a**, **2j**, **2p** and **3a**.

*4.1.4.1. N-(3-cyano-1H-indol-5-yl)isonicotinamide (**2a**).* A gray powder, yield 78.8%. ^{1}H NMR (600 MHz, DMSO-d_6) δ 12.21 (s, 1H), 10.54 (s, 1H), 8.79 (dd, J = 4.5, 1.5 Hz, 2H), 8.24 (s, 1H), 8.22 (d, J = 1.6 Hz, 1H), 7.90 (dd, J = 4.5, 1.5 Hz, 2H), 7.65 (dd, J = 8.8, 1.8 Hz, 1H), 7.56 (d, J = 8.8 Hz, 1H). ^{13}C NMR (125 MHz, DMSO-d_6) δ 164.26, 150.73, 142.51, 135.42, 133.70, 132.67, 127.35, 122.03, 118.16, 116.84, 113.49, 110.24, 84.78. ESI-HRMS calcd. for $C_{15}H_{10}N_4O$ $[M-H]^-$ 261.0776, found:261.0792.

*4.1.4.2. N-(3-cyano-1H-indol-5-yl)-2-chloroisonicotinamide (**2j**).* A brown powder, yield 69.7%. ^{1}H NMR (500 MHz, DMSO-d_6) δ 12.23 (s, 1H), 10.61 (s, 1H), 8.62 (d, J = 4.6 Hz, 1H), 8.25 (s, 1H), 8.20 (s, 1H), 8.03 (s, 1H), 7.91 (d, J = 4.2 Hz, 1H), 7.64 (d, J = 8.7 Hz, 1H), 7.56 (d, J = 8.7 Hz, 1H). ^{13}C NMR (125 MHz, DMSO-d_6) δ 162.08, 150.69, 150.51, 145.41, 134.82, 132.82, 132.13, 126.71, 122.08, 121.08, 117.46, 116.14, 112.89, 109.68, 84.20. ESI-HRMS calcd. for $C_{15}H_9ClN_4O$ $[M-H]^-$ 295.0387, found: 295.0408.

*4.1.4.3. N-(3-cyano-1H-indol-5-yl)-2-fluoroisonicotinamide (**2p**).* A brown powder, yield 72.6%. ^{1}H NMR (500 MHz, DMSO-d_6) δ 12.23 (s, 1H), 10.61 (s, 1H), 8.46 (d, J = 4.9 Hz, 1H), 8.26 (s, 1H), 8.21 (s, 1H), 7.87 (d, J = 4.2 Hz, 1H), 7.70 (s, 1H), 7.63 (d, J = 8.8 Hz, 1H), 7.57 (d, J = 8.7 Hz, 1H). ^{13}C NMR (125 MHz, DMSO-d_6) δ 163.24 (d, J = 235.8 Hz), 162.18 (d, J = 3.7 Hz), 148.29 (d, J = 14.9 Hz), 147.98 (d, J = 7.4 Hz), 134.84, 132.80, 132.13, 126.71, 120.04 (d, J = 4.0 Hz), 117.49, 116.15, 112.91, 109.69, 107.83 (d, J = 39.5 Hz), 84.19. ESI-HRMS calcd. for $C_{15}H_9FN_4O$ $[M-H]^-$ 279.0682, found:279.0691.

*4.1.4.4. N-(3-cyano-1H-indol-5-yl)-1H-benzo[d]imidazole-5-carboxamide (**3a**).* A gray solid, yield 74.7%. ^{1}H NMR (500 MHz, DMSO-d_6) δ 12.71 (s, 1H), 12.15 (s, 1H), 10.27 (s, 1H), 8.44 (s, 1H), 8.38 (s, 1H), 8.26 (s, 1H), 8.22 (s, 1H), 7.90 (s, 1H), 7.80–7.62 (m, 2H), 7.53 (d, J = 8.7 Hz, 1H). ^{13}C NMR (125 MHz, DMSO-d_6) δ 165.68, 143.89, 139.60, 136.46, 134.44, 134.00, 131.68, 128.40, 126.78, 121.65, 117.64, 116.32, 115.48, 114.30, 112.61, 109.30, 84.07. ESI-HRMS calcd. for $C_{17}H_{11}N_5O$ $[M-H]^-$ 300.0885, found:300.0896.

*4.1.5. General procedure for the synthesis of N-(1-alkyl-3-cyano-1H-indol-5-yl)isonicotinamides **2b-i**, N-(1-alkyl-3-cyano-1H-indol-5-yl)-2-chloroisonicotinamides **2k-o** and N-(1-alkyl-3-cyano-1H-indol-5-yl)-2-fluoroisonicotinamides **2q-w***

To a cooled solution of compound **7** (0.76 mmol) in anhydrous DMF (10 mL) was added NaH (1.91 mmol as 60% dispersion in paraffin oil) and kept at −5 °C for 30 min. Then, alkyl chloride/bromide (0.92 mmol), and potassium iodide (0.05 mmol) were successively added. The mixture was stirred under nitrogen atmosphere at 60 °C overnight. After the completion of the reaction, the insoluble solid was filtered out and the filtrate was diluted with water (200 mL). The formed precipitate was collected, washed with water and dried to yield a crude product, which was further purified by recrystallization from 50% ethanol to provide corresponding products **2b-i**, **2 k-o** and **2q-w**.

*4.1.5.1. N-(3-cyano-1-methyl-1H-indol-5-yl)isonicotinamide (**2b**).* A white powder, yield 88.7%. ^{1}H NMR (600 MHz, DMSO-d_6) δ 10.56 (s, 1H), 8.80 (d, J = 5.1 Hz, 2H), 8.23 (s, 1H), 8.22 (d, J = 1.5 Hz, 1H), 7.90 (d, J = 5.9 Hz, 2H), 7.70 (dd, J = 8.9, 1.8 Hz, 1H), 7.64 (d, J = 8.9 Hz, 1H), 3.87 (s, 3H). ^{13}C NMR (125 MHz, DMSO-d_6) δ 164.30, 150.75, 142.44, 138.51, 134.01, 133.38, 127.67, 122.03, 118.03, 116.51, 112.10, 110.35, 83.58, 33.94. ESI-HRMS calcd. for $C_{16}H_{12}N_4O$ $[M-H]^-$ 275.0933, found: 275.0959.

*4.1.5.2. N-(3-cyano-1-ethyl-1H-indol-5-yl)isonicotinamide (**2c**).* A white powder, yield 85.5%. ^{1}H NMR (500 MHz, DMSO-d_6) δ 10.55 (s, 1H), 8.80 (d, J = 3.5 Hz, 2H), 8.31 (s, 1H), 8.22 (s, 1H), 7.90 (d, J = 4.0 Hz, 2H), 7.69 (s, 2H), 4.28 (q, J = 7.0 Hz, 2H), 1.41 (t, J = 7.1 Hz, 3H). ^{13}C NMR (125 MHz, DMSO) δ 163.65, 150.11, 141.81, 136.45, 133.35, 131.82, 127.22, 121.37, 117.44, 115.86, 111.44, 109.92, 83.28, 41.31, 14.89. ESI-HRMS calcd. for $C_{17}H_{14}N_4O$ $[M-H]^-$ 289.1089, found: 289.1077.

*4.1.5.3. N-(3-cyano-1-propyl-1H-indol-5-yl)isonicotinamide (**2d**).* A white powder, yield 89.7%. ^{1}H NMR (600 MHz, DMSO-d_6) δ 10.56 (s, 1H), 8.80 (d, J = 5.2 Hz, 2H), 8.30 (s, 1H), 8.22 (d, J = 0.8 Hz, 1H), 7.90 (d, J = 5.8 Hz, 2H), 7.71 (d, J = 8.9 Hz, 1H), 7.68 (dd, J = 8.9, 1.5 Hz, 1H), 4.21 (t, J = 7.0 Hz, 2H), 1.84–1.78 (m, 2H), 0.84 (t, J = 7.4 Hz, 3H). ^{13}C NMR (125 MHz, DMSO-d_6) δ 164.29, 150.75, 142.43, 137.73, 133.95, 132.76, 127.75, 122.02, 118.05, 116.54, 112.24, 110.48, 83.81, 48.47, 23.28, 11.38. ESI-HRMS calcd. for $C_{18}H_{16}N_4O$ $[M-H]^-$ 303.1246, found: 303.1259.

*4.1.5.4. N-(3-cyano-1-isopropyl-1H-indol-5-yl)isonicotinamide (**2e**).* A white powder, yield 84.6%. ^{1}H NMR (500 MHz, DMSO-d_6) δ 10.55 (s, 1H), 8.80 (d, J = 4.6 Hz, 2H), 8.42 (s, 1H), 8.22 (s, 1H), 7.90 (d, J = 4.5 Hz, 2H), 7.74 (d, J = 8.9 Hz, 1H), 7.69 (d, J = 8.9 Hz, 1H), 4.86–4.81 (m, 1H), 1.49 (d, J = 6.6 Hz, 6H). ^{13}C NMR (125 MHz, DMSO-d_6) δ 163.65, 150.10, 141.81, 133.93, 133.35, 131.61, 127.21, 121.37, 117.38, 115.93, 111.58, 109.92, 83.65, 48.06, 22.03. ESI-HRMS calcd. for $C_{18}H_{16}N_4O$ $[M-H]^-$ 303.1246, found: 303.1224.

*4.1.5.5. N-(1-allyl-3-cyano-1H-indol-5-yl)isonicotinamide (**2f**).* A light yellow powder, yield 76.6%. ^{1}H NMR (500 MHz, DMSO-d_6) δ 10.55 (s, 1H), 8.80 (d, J = 3.6 Hz, 2H), 8.27 (s, 1H), 8.23 (s, 1H), 7.90 (d, J = 4.2 Hz, 2H), 7.68 (d, J = 8.8 Hz, 1H), 7.63 (d, J = 8.8 Hz, 1H), 6.06–6.02 (m, 1H), 5.22 (d, J = 10.2 Hz, 1H), 5.10 (d, J = 17.1 Hz, 1H), 4.92 (d, J = 4.6 Hz, 2H). ^{13}C NMR (125 MHz, DMSO-d_6) δ 163.68, 150.11, 141.80, 137.09, 133.45, 133.00, 132.07, 127.19, 121.37, 117.72, 117.57, 115.69, 111.75, 109.94, 83.68, 48.74. ESI-HRMS calcd. for $C_{18}H_{14}N_4O$ $[M-H]^-$ 301.1089, found: 301.1084.

*4.1.5.6. N-(3-cyano-1-(prop-2-yn-1-yl)-1H-indol-5-yl)isonicotinamide (**2g**).* A yellow powder, yield 73.4%. ^{1}H NMR (600 MHz, DMSO-d_6) δ 10.62 (s, 1H), 8.80 (d, J = 5.6 Hz, 2H), 8.30 (s, 1H), 8.27 (d, J = 1.5 Hz, 1H), 7.90 (dd, J = 7.2, 4.9 Hz, 3H), 7.76–7.71 (m, 2H), 5.89 (d, J = 6.5 Hz, 2H). ^{13}C NMR (150 MHz, DMSO-d_6) δ 202.81, 164.41, 150.75, 142.34, 135.40, 134.78, 131.74, 128.16, 122.03, 118.63, 115.69, 112.77, 110.56, 97.43, 89.85, 86.96. ESI-HRMS calcd. for $C_{18}H_{12}N_4O$ $[M-H]^-$ 299.0933, found: 299.0952.

*4.1.5.7. N-(1-benzyl-3-cyano-1H-indol-5-yl)isonicotinamide (**2h**).* A light yellow powder, yield 70.5%. ^{1}H NMR (500 MHz, DMSO-d_6) δ 10.54 (s, 1H), 8.79 (d, J = 4.5 Hz, 2H), 8.45 (s, 1H), 8.23 (s, 1H), 7.89 (d, J = 4.4 Hz, 2H), 7.65 (s, 2H), 7.33 (d, J = 6.9 Hz, 2H), 7.29 (d, J = 6.5 Hz, 3H), 5.52 (s, 2H). ^{13}C NMR (125 MHz, DMSO-d_6) δ 163.68, 150.10, 141.78, 137.42, 136.49, 133.50, 132.03, 128.57, 127.67, 127.32, 127.08, 121.36, 117.67, 115.64, 111.87, 109.98, 83.93, 49.85. ESI-HRMS calcd. for $C_{22}H_{16}N_4O$ $[M-H]^-$ 351.1246, found: 351.1231.

*4.1.5.8. N-(3-cyano-1-cyclopentyl-1H-indol-5-yl)isonicotinamide (**2i**).* A white powder, yield 68.4%. ^{1}H NMR (500 MHz, DMSO-d_6) δ 10.55 (s, 1H), 8.80 (d, J = 4.2 Hz, 2H), 8.38 (s, 1H), 8.21 (s, 1H), 7.90 (d, J = 4.4 Hz, 2H), 7.73 (d, J = 8.9 Hz, 1H), 7.69 (d, J = 9.0 Hz, 1H), 4.96–4.92 (m, 1H), 2.20 (d, J = 7.7 Hz, 2H), 1.91–1.85 (m, 4H), 1.72 (s, 2H). ^{13}C NMR (125 MHz, DMSO-d_6) δ 163.64, 150.09, 141.82, 134.33, 133.41, 132.25, 127.31, 121.37, 117.38, 115.92, 111.84, 109.86, 83.61, 57.37, 31.85, 23.30. ESI-HRMS calcd. for $C_{20}H_{18}N_4O$ $[M-H]^-$ 329.1402, found: 329.1390.

*4.1.5.9. N-(3-cyano-1-methyl −1H-indol-5-yl)-2-chloroisonicotinamide (**2k**).* A white powder, yield 87.7%. ^{1}H NMR (500 MHz, DMSO-d_6) δ 10.62 (s, 1H), 8.63 (d, J = 4.8 Hz, 1H), 8.24 (s, 1H), 8.20 (s, 1H), 8.03 (s, 1H), 7.91 (d, J = 4.6 Hz, 1H), 7.69 (d, J = 8.8 Hz, 1H), 7.65 (d, J = 8.8 Hz, 1H), 3.87 (s, 3H). ^{13}C NMR (125 MHz, DMSO-d_6) δ 162.12, 150.70, 150.53, 145.35, 137.92, 133.14, 132.84, 127.03, 122.07, 121.08, 117.33, 115.80, 111.49, 109.79, 83.01, 33.31. ESI-HRMS calcd. for $C_{16}H_{11}ClN_4O$ [M−H]$^-$ 309.0543, found: 309.0577.

*4.1.5.10. N-(3-cyano-1-ethyl −1H-indol-5-yl)-2-chloroisonicotinamide (**2l**).* A white powder, yield 88.2%. ^{1}H NMR (500 MHz, DMSO-d_6) δ 10.62 (s, 1H), 8.63 (d, J = 5.0 Hz, 1H), 8.32 (s, 1H), 8.20 (s, 1H), 8.03 (s, 1H), 7.91 (d, J = 4.2 Hz, 1H), 7.69 (q, J = 8.9 Hz, 2H), 4.28 (q, J = 7.1 Hz, 2H), 1.41 (t, J = 7.2 Hz, 3H). ^{13}C NMR (125 MHz, DMSO-d_6) δ 162.10, 150.70, 150.53, 145.33, 136.53, 133.11, 131.89, 127.20, 122.07, 121.08, 117.34, 115.83, 111.49, 109.94, 83.30, 41.32, 14.90. ESI-HRMS calcd. for $C_{17}H_{13}ClN_4O$ [M−H]$^-$ 323.0700, found: 323.0712.

*4.1.5.11. N-(3-cyano-1- propyl −1H-indol-5-yl)-2-chloroisonicotinamide (**2 m**).* A white powder, yield 85.1%. ^{1}H NMR (500 MHz, DMSO-d_6) δ 10.61 (s, 1H), 8.63 (d, J = 4.8 Hz, 1H), 8.30 (s, 1H), 8.20 (s, 1H), 8.03 (s, 1H), 7.91 (d, J = 4.8 Hz, 1H), 7.71 (d, J = 8.9 Hz, 1H), 7.67 (d, J = 8.9 Hz, 1H), 4.21 (t, J = 6.9 Hz, 2H), 1.86–1.76 (m, 2H), 0.84 (t, J = 7.2 Hz, 3H). ^{13}C NMR (125 MHz, DMSO-d_6) δ 162.10, 150.70, 150.54, 145.33, 137.14, 133.07, 132.21, 127.11, 122.07, 121.08, 117.34, 115.84, 111.64, 109.91, 83.23, 47.85, 22.64, 10.74. ESI-HRMS calcd. for $C_{18}H_{15}ClN_4O$ [M−H]$^-$ 337.0856, found: 337.0868.

*4.1.5.12. N-(3-cyano-1- isopropyl −1H-indol-5-yl)-2-chloroisonicotinamide (**2n**).* A white powder, yield 87.7%. ^{1}H NMR (500 MHz, DMSO-d_6) δ 10.63 (s, 1H), 8.63 (d, J = 4.9 Hz, 1H), 8.44 (s, 1H), 8.21 (s, 1H), 8.04 (s, 1H), 7.91 (d, J = 4.9 Hz, 1H), 7.75 (d, J = 8.9 Hz, 1H), 7.67 (d, J = 9.0 Hz, 1H), 4.86–4.81 (m, 1H), 1.49 (d, J = 6.5 Hz, 6H). ^{13}C NMR (125 MHz, DMSO-d_6) δ 162.10, 150.70, 150.54, 145.33, 134.04, 133.11, 131.66, 127.16, 122.07, 121.09, 117.27, 115.92, 111.65, 109.92, 83.65, 48.05, 22.04. ESI-HRMS calcd. for $C_{18}H_{15}ClN_4O$ [M−H]$^-$ 337.0856, found: 337.0869.

*4.1.5.13. N-(1-allyl-3-cyano-1H-indol-5-yl)-2-chloroisonicotinamide (**2o**).* A light yellow powder, yield 81.2%. ^{1}H NMR (500 MHz, DMSO-d_6) δ 10.64 (s, 1H), 8.63 (d, J = 4.9 Hz, 1H), 8.28 (s, 1H), 8.22 (s, 1H), 8.04 (s, 1H), 7.91 (d, J = 4.8 Hz, 1H), 7.65 (q, J = 8.9 Hz, 2H), 6.06–6.00 (m, 1H), 5.22 (d, J = 10.1 Hz, 1H), 5.09 (d, J = 17.3 Hz, 1H), 4.92 (d, J = 5.0 Hz, 2H). ^{13}C NMR (125 MHz, DMSO-d_6) δ 162.14, 150.70, 150.54, 145.33, 137.19, 133.20, 133.00, 132.13, 127.16, 122.08, 121.08, 117.72, 117.46, 115.67, 111.82, 109.95, 83.69, 48.74. ESI-HRMS calcd. for $C_{18}H_{13}ClN_4O$ [M−H]$^-$ 335.0700, found: 335.0709.

*4.1.5.14. N-(3-cyano-1-ethyl-1H-indol-5-yl)-2-fluoroisonicotinamide (**2q**).* A white powder, yield 86.5%. ^{1}H NMR (500 MHz, DMSO-d_6) δ 10.64 (s, 1H), 8.46 (d, J = 3.7 Hz, 1H), 8.32 (s, 1H), 8.21 (s, 1H), 7.87 (s, 1H), 7.75–7.64 (m, 3H), 4.31–4.25 (m, 2H), 1.41 (t, J = 6.7 Hz, 3H). ^{13}C NMR (125 MHz, DMSO-d_6) δ 163.25 (d, J = 236.2 Hz), 162.20 (d, J = 3.2 Hz), 148.29 (d, J = 14.8 Hz), 147.89 (d, J = 7.6 Hz), 136.54, 133.09, 131.89, 127.20, 120.03 (d, J = 4.0 Hz), 117.37, 115.84, 111.51, 109.96, 107.83 (d, J = 39.8 Hz), 83.29, 41.32, 14.90. ESI-HRMS calcd. for $C_{17}H_{13}FN_4O$ [M−H]$^-$ 307.0995, found: 307.1023.

*4.1.5.15. N-(3-cyano-1-propyl-1H-indol-5-yl)-2-fluoroisonicotinamide (**2r**).* A white powder, yield 76.5%. ^{1}H NMR (500 MHz, DMSO-d_6) δ 10.62 (s, 1H), 8.46 (d, J = 4.9 Hz, 1H), 8.31 (s, 1H), 8.21 (s, 1H), 7.87 (d, J = 4.2 Hz, 1H), 7.74–7.65 (m, 3H), 4.22 (t, J = 6.9 Hz, 2H), 1.85–1.77 (m, 2H), 0.84 (t, J = 7.3 Hz, 3H). ^{13}C NMR (125 MHz, DMSO-d_6) δ 163.25 (d, J = 236.3 Hz), 162.19 (d, J = 3.9 Hz), 148.30 (d, J = 14.8 Hz), 147.89 (d, J = 7.6 Hz), 137.13, 133.05, 132.23, 127.12, 120.02 (d, J = 4.0 Hz), 117.38, 115.82, 111.64, 109.94, 107.83 (d, J = 39.1 Hz), 83.24, 47.85, 22.64, 10.73. ESI-HRMS calcd. for $C_{18}H_{15}FN_4O$ [M−H]$^-$ 321.1152, found: 321.1160.

*4.1.5.16. N-(3-cyano-1-isopropyl-1H-indol-5-yl)-2-fluoroisonicotinamide (**2 s**).* A white powder, yield 78.5%. ^{1}H NMR (500 MHz, DMSO-d_6) δ 10.62 (s, 1H), 8.49–8.40 (m, 2H), 8.21 (s, 1H), 7.87 (d, J = 4.1 Hz, 1H), 7.78–7.65 (m, 3H), 4.84 (dt, J = 12.9, 6.4 Hz, 1H), 1.49 (d, J = 6.5 Hz, 6H). ^{13}C NMR (125 MHz, DMSO-d_6) δ 163.25 (d, J = 235.9 Hz), 162.19 (d, J = 3.8 Hz), 148.31 (d, J = 15.1 Hz), 147.89 (d, J = 7.0 Hz), 134.05, 133.09, 131.67, 127.17, 120.03 (d, J = 4.0 Hz), 117.30, 115.92, 111.66, 109.94, 107.83 (d, J = 39.8 Hz), 83.65, 48.05, 22.04. ESI-HRMS calcd. for $C_{18}H_{15}FN_4O$ [M−H]$^-$ 321.1152, found: 321.1175.

*4.1.5.17. N-(1-allyl-3-cyano-1H-indol-5-yl)-2-fluoroisonicotinamide (**2 t**).* A light yellow powder, yield 73.4%. ^{1}H NMR (500 MHz, DMSO-d_6) δ 10.63 (s, 1H), 8.46 (d, J = 4.9 Hz, 1H), 8.28 (s, 1H), 8.23 (s, 1H), 7.87 (d, J = 4.5 Hz, 1H), 7.70 (s, 1H), 7.66 (q, J = 9.0 Hz, 2H), 6.05–6.01 (m, 1H), 5.22 (d, J = 10.2 Hz, 1H), 5.10 (d, J = 17.1 Hz, 1H), 4.92 (d, J = 5.0 Hz, 2H). ^{13}C NMR (125 MHz, DMSO-d_6) δ 163.24 (d, J = 236.5 Hz), 162.23 (d, J = 3.7 Hz), 148.31 (d, J = 14.9 Hz), 147.88 (d, J = 7.8 Hz), 137.20, 133.18, 133.00, 132.14, 127.16, 120.03 (d, J = 4.0 Hz), 117.72, 117.49, 115.67, 111.83, 109.97, 107.84 (d, J = 39.1 Hz), 83.68, 48.74. ESI-HRMS calcd. for $C_{18}H_{13}FN_4O$ [M−H]$^-$ 319.0995, found: 319.1012.

*4.1.5.18. N-(3-cyano-1-(prop-2-yn-1-yl)-1H-indol-5-yl)-2-fluoroisonicotinamide (**2u**).* A yellow powder, yield 74.5%. ^{1}H NMR (500 MHz, DMSO-d_6) δ 10.68 (s, 1H), 8.46 (d, J = 5.0 Hz, 1H), 8.33 (d, J = 8.2 Hz, 1H), 8.26 (s, 1H), 7.92 (d, J = 9.0 Hz, 1H), 7.87 (d, J = 4.5 Hz, 1H), 7.77–7.69 (m, 3H), 5.90 (d, J = 6.5 Hz, 2H). ^{13}C NMR (125 MHz, DMSO-d_6) δ 202.20, 163.25 (d, J = 230.2 Hz), 162.30 (d, J = 2.5 Hz), 148.32 (d, J = 14.8 Hz), 147.80 (d, J = 6.9 Hz), 134.84, 133.88, 131.22, 127.53, 120.04 (d, J = 4.1 Hz), 117.98, 114.98, 112.19, 110.03, 107.85 (d, J = 39.6 Hz), 96.78, 89.21, 86.36. ESI-HRMS calcd. for $C_{18}H_{11}FN_4O$ [M−H]$^-$ 317.0839, found: 317.0864.

*4.1.5.19. N-(1-benzyl-3-cyano-1H-indol-5-yl)-2-fluoroisonicotinamide (**2v**).* A light yellow powder, yield 68.8%. ^{1}H NMR (500 MHz, DMSO-d_6) δ 10.69 (s, 1H), 8.50–8.43 (m, 2H), 8.23 (s, 1H), 7.87 (s, 1H), 7.73–7.60 (m, 3H), 7.33 (d, J = 6.9 Hz, 2H), 7.29 (d, J = 6.4 Hz, 3H), 5.52 (s, 2H). ^{13}C NMR (125 MHz, DMSO-d_6) δ 163.23 (d, J = 236.6 Hz), 162.25 (d, J = 3.9 Hz), 148.30 (d, J = 14.8 Hz), 147.88 (d, J = 6.9 Hz), 137.53, 136.49, 133.27, 132.08, 128.58, 127.68, 127.28, 127.09, 120.05 (d, J = 4.0 Hz), 117.61, 115.64, 111.96, 110.00, 107.85 (d, J = 39.0 Hz), 83.90, 49.82. ESI-HRMS calcd. for $C_{22}H_{15}FN_4O$ [M−H]$^-$ 369.1152, found: 369.1174.

*4.1.5.20. N-(3-cyano-1-cyclopentyl-1H-indol-5-yl)-2-fluoroisonicotinamide (**2w**).* A white powder, yield 65.4%. ^{1}H NMR (500 MHz, DMSO-d_6) δ 10.62 (s, 1H), 8.46 (d, J = 4.8 Hz, 1H), 8.40 (s, 1H), 8.21 (s, 1H), 7.87 (d, J = 3.3 Hz, 1H), 7.74 (d, J = 8.9 Hz, 1H), 7.72–7.65 (m, 2H), 4.99–4.92 (m, 1H), 2.19 (d, J = 7.9 Hz, 2H), 1.87 (d, J = 16.1 Hz, 4H), 1.71 (s, 2H). ^{13}C NMR (125 MHz, DMSO-d_6) δ 163.25 (d, J = 235.7 Hz), 162.18 (d, J = 3.8 Hz), 148.30 (d, J = 14.8 Hz), 147.88 (d, J = 6.9 Hz), 134.44, 133.14, 132.31, 127.28, 120.02 (d, J = 4.0 Hz), 117.30, 115.91, 111.91, 109.89, 107.82 (d, J = 39.9 Hz), 83.61, 57.35, 31.85, 23.28. ESI-HRMS calcd. for $C_{20}H_{17}FN_4O$ [M−H]$^-$ 347.1308, found: 347.1329.

4.1.6. General procedure for the synthesis of 1-alkyl-5-nitro-1H-indole-3-carbonitrile (7)

To a cooled solution of compound **5** (1.00 g, 5.34 mmol) in anhydrous DMF (15 mL) was added NaH (0.53 g, 13.36 mmol as 60% dispersion in paraffin oil) and kept at −5 °C for 30 min. Alkyl chloride/bromide (6.41 mmol), and potassium iodide (0.05 mmol) was then

added. The mixture was stirred under nitrogen atmosphere at 60 °C overnight. After the completion of the reaction, the insoluble solid was filtered out and the filtrate was diluted with water (250 mL). The formed precipitate was collected, washed with water and dried to provide corresponding key intermediates 1- alkyl-5-nitro-1*H*-indole-3-carbonitrile **7a-h**.

*4.1.6.1. 1-methyl-5-nitro-1H-indole-3-carbonitrile (**7a**).* A yellow solid, yield 92.1%. ^{1}H NMR (500 MHz, DMSO-d_6) δ 8.50 (s, 1H), 8.43 (s, 1H), 8.16 (d, J = 9.1 Hz, 1H), 7.84 (d, J = 9.1 Hz, 1H), 3.93 (s, 3H). ^{13}C NMR (125 MHz, DMSO-d_6) δ 142.51, 141.36, 138.53, 126.02, 118.28, 114.98, 114.38, 112.33, 85.65, 33.79.

*4.1.6.2. 1-ethyl-5-nitro-1H-indole-3-carbonitrile (**7b**).* A yellow solid, yield 89.3%. ^{1}H NMR (500 MHz, DMSO-d_6) δ 8.61 (s, 1H), 8.43 (s, 1H), 8.15 (d, J = 9.1 Hz, 1H), 7.92 (d, J = 9.1 Hz, 1H), 4.36 (q, J = 7.1 Hz, 2H), 1.41 (t, J = 7.2 Hz, 3H). ^{13}C NMR (125 MHz, DMSO-d_6) δ 142.47, 140.03, 137.65, 126.17, 118.27, 115.11, 114.41, 112.26, 85.97, 41.85, 14.81.

*4.1.6.3. 1-propyl-5-nitro-1H-indole-3-carbonitrile (**7c**).* A yellow solid, yield 85.5%. ^{1}H NMR (500 MHz, DMSO-d_6) δ 8.61 (s, 1H), 8.47 (s, 1H), 8.17 (d, J = 8.7 Hz, 1H), 7.96 (d, J = 9.1 Hz, 1H), 4.31 (t, J = 6.8 Hz, 2H), 1.82 (dd, J = 14.2, 7.1 Hz, 2H), 0.84 (t, J = 7.2 Hz, 3H). ^{13}C NMR (125 MHz, DMSO-d_6) δ 142.54, 140.57, 138.06, 126.13, 118.33, 115.17, 114.41, 112.45, 86.00, 48.25, 22.63, 10.64.

*4.1.6.4. 1-isopropyl-5-nitro-1H-indole-3-carbonitrile (**7d**).* A yellow solid, yield 83.4%. ^{1}H NMR (500 MHz, DMSO-d_6) δ 8.75 (s, 1H), 8.43 (s, 1H), 8.14 (d, J = 9.2 Hz, 1H), 7.96 (d, J = 9.2 Hz, 1H), 5.01–4.92 (m, 1H), 1.50 (d, J = 6.6 Hz, 6H). ^{13}C NMR (125 MHz, DMSO-d_6) δ 142.49, 137.51, 137.42, 126.15, 118.19, 115.09, 114.45, 112.34, 86.45, 48.78, 21.95.

*4.1.6.5. 1-allyl-5-nitro-1H-indole-3-carbonitrile (**7e**).* A yellow solid, yield 81.4%. ^{1}H NMR (500 MHz, DMSO-d_6) δ 8.58 (s, 1H), 8.50 (s, 1H), 8.18 (d, J = 9.4 Hz, 1H), 7.86 (d, J = 9.2 Hz, 1H), 6.11–5.97 (m, 1H), 5.24 (d, J = 10.3 Hz, 1H), 5.09 (d, J = 17.1 Hz, 1H), 5.02 (d, J = 5.1 Hz, 2H). ^{13}C NMR (125 MHz, DMSO-d_6) δ 142.66, 140.66, 137.93, 132.50, 126.23, 118.48, 118.12, 115.23, 114.29, 112.62, 86.32, 49.09.

*4.1.6.6. 5-nitro-1-(prop-2-yn-1-yl)-1H-indole-3-carbonitrile (**7f**).* A yellow solid, yield 76.4%. ^{1}H NMR (500 MHz, DMSO-d_6) δ 8.57 (s, 1H), 8.46 (s, 1H), 8.21 (d, J = 9.1 Hz, 1H), 7.91 (d, J = 9.1 Hz, 1H), 5.37 (d, J = 5.9 Hz, 1H), 5.31 (s, 2H). ^{13}C NMR (125 MHz, DMSO-d_6) δ 142.91, 140.10, 137.53, 126.31, 118.77, 115.32, 114.03, 112.59, 86.82, 77.26, 66.45, 36.56.

*4.1.6.7. 1-benzyl-5-nitro-1H-indole-3-carbonitrile (**7 g**).* A yellow solid, yield 73.8%. ^{1}H NMR (500 MHz, DMSO-d_6) δ 8.77 (s, 1H), 8.51 (s, 1H), 8.17 (d, J = 9.0 Hz, 1H), 7.91 (d, J = 9.1 Hz, 1H), 7.34 (d, J = 5.7 Hz, 2H), 7.31 (s, 3H), 5.63 (s, 2H). ^{13}C NMR (125 MHz, DMSO-d_6) δ 142.73, 140.91, 137.90, 135.88, 128.69, 127.91, 127.18, 126.37, 118.63, 115.32, 114.28, 112.70, 86.57, 50.17.

*4.1.6.8. 1-cyclopentyl-5-nitro-1H-indole-3-carbonitrile (**7 h**).* A yellow solid, yield 80.5%. ^{1}H NMR (500 MHz, DMSO-d_6) δ 8.71 (s, 1H), 8.45 (s, 1H), 8.16 (d, J = 9.1 Hz, 1H), 7.96 (d, J = 9.1 Hz, 1H), 5.13–5.02 (m, 1H), 2.22 (d, J = 7.1 Hz, 2H), 1.87 (d, J = 11.7 Hz, 4H), 1.72 (s, 2H). ^{13}C NMR (125 MHz, DMSO-d_6) δ 142.52, 138.08, 137.92, 126.24, 118.23, 115.07, 114.50, 112.62, 86.37, 57.79, 31.94, 23.28.

*4.1.7. General procedure for the synthesis of N-(1-alkyl-3-cyano-1H-indol-5-yl)-1H-benzo[d]imidazole-5-carboxamides **3b-i***

A solution of compound **7** (2.50 mmol), tin chloride dihydrate (5.63 g, 25.0 mmol) and hydrochloric acid (5 mL) in ethanol (50 mL) and water (5 mL) was heated at 60 °C overnight. After the completion of the reaction, the solution was basified with an aqueous solution of sodium hydroxide and extracted with ethyl acetate (100 mL*3). The ethyl acetate extracts were combined, dried over sodium sulfate, and evaporated to dryness to provide corresponding key intermediates 5-amino-1- alkyl −1*H*-indole-3-carbonitrile **8a-h**, which was directly used in the next step without further purification. Into a solution of compound **9** (1.17 mmol) and triethylamine (0.35 g, 3.50 mmol) in tetrahydrofuran (50 mL) at −5 °C, was added 1*H*-benzo[*d*]imidazole-5-carbonyl chloride (0.32 g, 1.75 mmol). The mixture was maintained at the same temperature for 1 h and then stirred at room temperature overnight. After the completion of the reaction, the insoluble materials were removed by filtration and washed with THF. The filtrate was evaporated in vacuum to give crude products, which were then purified using column chromatography to obtain the pure corresponding products **3b-i**.

*4.1.7.1. N-(3-cyano-1-methyl-1H-indol-5-yl)-1H-benzo[d]imidazole-5-carboxamide (**3b**).* A brown powder, yield 78.7%. ^{1}H NMR (500 MHz, DMSO-d_6) δ 12.78 (s, 1H), 10.32 (s, 1H), 8.39 (s, 1H), 8.35 (s, 1H), 8.28 (s, 1H), 8.21 (s, 1H), 7.90 (d, J = 7.8 Hz, 1H), 7.76 (d, J = 8.4 Hz, 1H), 7.71 (d, J = 8.0 Hz, 1H), 7.62 (d, J = 8.5 Hz, 1H), 3.87 (s, 3H). ^{13}C NMR (125 MHz, DMSO-d_6) δ 165.71, 143.91, 139.85, 138.42, 137.56, 134.34, 132.40, 128.48, 127.10, 121.69, 117.48, 116.01, 115.63, 114.20, 111.22, 109.37, 82.85, 33.26. ESI-HRMS calcd. for $C_{18}H_{13}N_5O$ [M−H]$^-$ 314.1042, found:314.1059.

*4.1.7.2. N-(3-cyano-1-ethyl-1H-indol-5-yl)-1H-benzo[d]imidazole-5-carboxamide (**3c**).* A gray powder, yield 76.3%. ^{1}H NMR (500 MHz, DMSO-d_6) δ 12.77 (s, 1H), 10.34 (s, 1H), 8.40 (s, 1H), 8.35 (s, 1H), 8.30 (d, J = 2.6 Hz, 2H), 7.91 (d, J = 8.4 Hz, 1H), 7.75–7.67 (m, 3H), 4.28 (q, J = 7.0 Hz, 2H), 1.41 (t, J = 7.1 Hz, 3H). ^{13}C NMR (125 MHz, DMSO-d_6) δ 165.71, 143.91, 139.72, 138.35, 136.18, 134.30, 131.43, 128.48, 127.26, 121.70, 117.49, 116.05, 115.69, 114.36, 111.25, 109.51, 83.12, 41.28, 14.93. ESI-HRMS calcd. for $C_{19}H_{15}N_5O$ [M−H]$^-$ 328.1198, found:328.1201.

*4.1.7.3. N-(3-cyano-1-propyl-1H-indol-5-yl)-1H-benzo[d]imidazole-5-carboxamide (**3d**).* An off-white powder, yield 78.1%. ^{1}H NMR (500 MHz, DMSO-d_6) δ 10.32 (s, 1H), 8.39 (s, 1H), 8.36 (s, 1H), 8.28 (d, J = 5.0 Hz, 2H), 7.91 (d, J = 8.3 Hz, 1H), 7.75–7.67 (m, 3H), 4.21 (t, J = 6.5 Hz, 2H), 1.82 (d, J = 7.0 Hz, 1H), 1.80 (d, J = 6.8 Hz, 1H), 0.84 (t, J = 7.1 Hz, 3H). ^{13}C NMR (125 MHz, DMSO-d_6) δ 165.72, 143.93, 139.66, 138.42, 136.77, 134.27, 131.77, 128.47, 127.19, 121.68, 117.52, 116.04, 115.66, 114.34, 111.36, 109.51, 83.08, 47.82, 22.64, 10.74. ESI-HRMS calcd. for $C_{20}H_{17}N_5O$ [M−H]$^-$ 342.1355, found:342.1375.

*4.1.7.4. N-(3-cyano-1-isopropyl-1H-indol-5-yl)-1H-benzo[d]imidazole-5-carboxamide (**3e**).* A gray powder, yield 74.2%. ^{1}H NMR (500 MHz, DMSO-d_6) δ 12.80 (s, 1H), 10.31 (s, 1H), 8.41 (s, 1H), 8.39 (s, 1H), 8.34 (s, 1H), 8.28 (s, 1H), 7.90 (d, J = 8.4 Hz, 1H), 7.76–7.68 (m, 3H), 4.86–4.81 (m, 1H), 1.50 (d, J = 6.5 Hz, 6H). ^{13}C NMR (125 MHz, DMSO-d_6) δ 165.69, 143.94, 139.64, 138.44, 134.30, 133.67, 131.21, 128.45, 127.22, 121.68, 117.39, 116.14, 115.61, 114.28, 111.40, 109.46, 83.46, 47.97, 22.06. ESI-HRMS calcd. for $C_{20}H_{17}N_5O$ [M−H]$^-$ 342.1355, found:342.1361.

*4.1.7.5. N-(1-allyl-3-cyano-1H-indol-5-yl)-1H-benzo[d]imidazole-5-carboxamide (**3f**).* A yellow powder, yield 76.1%. ^{1}H NMR (500 MHz, DMSO-d_6) δ 12.76 (s, 1H), 10.31 (s, 1H), 8.39 (s, 1H), 8.35 (s, 1H), 8.29 (s, 1H), 8.25 (s, 1H), 7.90 (d, J = 8.3 Hz, 1H), 7.74 (d, J = 8.9 Hz, 1H), 7.71 (d, J = 8.4 Hz, 1H), 7.61 (d, J = 8.9 Hz, 1H), 6.08–6.00 (m, 1H), 5.22 (d, J = 10.2 Hz, 1H), 5.10 (d, J = 17.1 Hz, 1H), 4.92 (d, J = 4.8 Hz, 2H). ^{13}C NMR (125 MHz, DMSO-d_6) δ 165.72, 143.90, 139.43, 138.33, 137.85, 136.85, 134.40, 133.09, 131.68, 128.31, 127.22, 121.69,

117.65, 117.59, 116.50, 114.41, 111.58, 109.51, 83.51, 48.71. ESI-HRMS calcd. for $C_{20}H_{15}N_5O$ $[M-H]^-$ 340.1198, found:340.1216.

*4.1.7.6. N-(3-cyano-1-(prop-2-yn-1-yl)-1H-indol-5-yl)-1H-benzo[d]imidazole-5-carboxamide (**3g**).* A yellow powder, yield 62.5%. ^{1}H NMR (500 MHz, DMSO-d_6) δ 12.89 (s, 1H), 10.35 (s, 1H), 8.41 (s, 1H), 8.35 (s, 1H), 8.30 (s, 2H), 7.91 (d, J = 7.9 Hz, 1H), 7.79 (d, J = 8.4 Hz, 1H), 7.70 (t, J = 8.6 Hz, 2H), 5.22 (s, 2H), 3.56 (s, 1H). ^{13}C NMR (125 MHz, DMSO-d_6) δ 165.72, 143.87, 139.41, 138.22, 136.42, 134.66, 131.32, 128.50, 127.24, 121.77, 117.80, 115.57, 115.49, 114.44, 111.52, 109.57, 84.15, 77.76, 76.62, 36.01. ESI-HRMS calcd. for $C_{20}H_{13}N_5O$ $[M-H]^-$ 338.1042, found:338.1057.

*4.1.7.7. N-(1-benzyl-3-cyano-1H-indol-5-yl)-1H-benzo[d]imidazole-5-carboxamide (**3h**).* A gray powder, yield 70.6%. ^{1}H NMR (500 MHz, DMSO-d_6) δ 10.31 (s, 1H), 8.44 (s, 1H), 8.36 (s, 1H), 8.33 (s, 1H), 8.29 (s, 1H), 7.87 (d, J = 8.2 Hz, 1H), 7.69 (d, J = 8.4 Hz, 2H), 7.62 (d, J = 8.6 Hz, 1H), 7.34 (d, J = 6.7 Hz, 2H), 7.29 (d, J = 6.5 Hz, 3H), 5.51 (s, 2H). ^{13}C NMR (125 MHz, DMSO-d_6) δ 165.78, 144.14, 139.71, 138.63, 137.14, 136.58, 134.48, 131.62, 128.57, 128.27, 127.65, 127.35, 127.09, 121.54, 117.71, 115.83, 115.65, 114.34, 111.67, 109.54, 83.76, 49.80. ESI-HRMS calcd. for $C_{24}H_{17}N_5O$ $[M-H]^-$ 390.1355, found:390.1375.

*4.1.7.8. N-(3-cyano-1-cyclopentyl-1H-indol-5-yl)-1H-benzo[d]imidazole-5-carboxamide (**3i**).* A brown powder, yield 70.6%. ^{1}H NMR (500 MHz, DMSO-d_6) δ 12.74 (s, 1H), 10.32 (s, 1H), 8.37 (s, 2H), 8.28 (s, 1H), 7.91 (s, 1H), 7.84–7.62 (m, 3H), 4.94 (d, J = 6.3 Hz, 1H), 2.19 (s, 2H), 1.86 (s, 4H), 1.71 (s, 2H). ^{13}C NMR (125 MHz, DMSO-d_6) δ 165.68, 143.92, 139.64, 138.55, 134.37, 134.09, 131.85, 128.50, 127.33, 122.28, 117.39, 116.13, 115.87, 114.31, 111.67, 109.40, 83.41, 57.29, 31.84, 23.29. ESI-HRMS calcd. for $C_{22}H_{19}N_5O$ $[M-H]^-$ 368.1511, found:368.1542.

*4.1.8. Synthesis of 1H-indol-5-amine (**9**)*

A mixture of 5-nitro-1*H*-indole (2.00 g, 12.33 mmol) and Pd/C (5%; 0.20 g) in ethanol (40 mL) under 40 psi of hydrogen atmosphere, was stirred at 25 °C for 18 h. After the completion of the reaction, the insoluble solid was filtered out. The filtrate was evaporated under reduced pressure to give 1*H*-indol-5-amine **9** (1.42 g yield 87.1%) as a light red solid. ^{1}H NMR (600 MHz, DMSO-d_6) δ 10.56 (s, 1H), 7.13 (t, J = 2.7 Hz, 1H), 7.10 (d, J = 8.5 Hz, 1H), 6.70 (d, J = 2.0 Hz, 1H), 6.51 (dd, J = 8.5, 2.1 Hz, 1H), 6.14 (dd, J = 3.4, 1.4 Hz, 1H), 4.42 (s, 2H). ^{13}C NMR (150 MHz, DMSO-d_6) δ 141.45, 130.26, 129.03, 125.20, 112.29, 111.86, 103.71, 100.09.

*4.1.9. Synthesis of N-(1H-indol-5-yl)isonicotinamide (**10**)*

Into a solution of compound **9** (1.00 g, 7.57 mmol) and triethylamine (2.30 g, 22.70 mmol) in tetrahydrofuran (80 mL) at −5 °C, was added isonicotinyl chloride (1.60 g, 11.35 mmol). The mixture was maintained at the same temperature for 1 h and then stirred at room temperature overnight. After the completion of the reaction, the insoluble materials were removed by filtration and washed with THF. The filtrate was evaporated in vacuum to remove about 3/4 of the solvent. The residue was dispersed into water, filtered under reduced pressure, washed and dried to give *N*-(1H-indol-5-yl)isonicotinamide **10** (1.37 g, yield 76.1%) as a white solid. ^{1}H NMR (600 MHz, DMSO-d_6) δ 11.07 (s, 1H), 10.33 (s, 1H), 8.78 (dd, J = 4.5, 1.5 Hz, 2H), 8.02 (s, 1H), 7.90 (dd, J = 4.5, 1.5 Hz, 2H), 7.44–7.38 (m, 2H), 7.35 (t, J = 2.7 Hz, 1H), 6.49–6.41 (m, 1H). ^{13}C NMR (150 MHz, DMSO-d_6) δ 163.94, 150.66, 142.91, 133.74, 130.86, 127.91, 126.54, 122.03, 116.50, 112.91, 111.64, 101.73.

*4.1.10. Synthesis of N-(3-formyl-1H-indol-5-yl)isonicotinamide (**11**)*

A mixture of anhydrous DMF (0.23 g, 3.16 mmol) and phosphorus oxychloride (0.97 g, 6.32 mmol) was stirred at 0 °C for 30 min. Then a solution of compound **10** (0.50 g, 2.11 mmol) in anhydrous DMF (2 mL) was added dropwise to the above mixture. After the addition, the mixture was stirred overnight at room temperature. Then, the reaction mixture was poured into ice water, basified with an aqueous solution of sodium hydroxide and refluxed for 1 h. After cooling, the precipitate was collected by filtration, washed with a large quantity of water and dried in vacuum to give *N*-(3-formyl-1H-indol-5-yl)isonicotinamide **11** (0.43 g, yield 76.9%) as a white solid. ^{1}H NMR (500 MHz, DMSO-d_6) δ 12.14 (s, 1H), 10.51 (s, 1H), 9.93 (s, 1H), 8.79 (d, J = 4.3 Hz, 2H), 8.55 (s, 1H), 8.29 (s, 1H), 7.91 (d, J = 4.4 Hz, 2H), 7.72 (d, J = 8.7 Hz, 1H), 7.51 (d, J = 8.7 Hz, 1H). ^{13}C NMR (125 MHz, DMSO-d_6) δ 184.62, 163.43, 150.05, 141.96, 138.88, 133.97, 133.37, 123.94, 121.40, 118.15, 117.72, 112.93, 112.06.

4.2. Assay of in vitro XO inhibitory activity

Bovine XO inhibitory potency *in vitro* was assayed spectrophotometrically by measuring the uric acid formation at 294 nm using a UV-2100 spectrophotometer (UNICO) at 25 °C. The testing method was based on the procedure reported by Matsumoto et al. [49] with modification. The assay mixture contained 0.1 M sodium pyrophosphate buffer (pH 8.3), 0.3 mM Na_2EDTA, 1 mM xanthine, 25 U/L XO (Sigma, X1875), and the test compound. The enzyme was pre-incubated for 10 min with the test compound, and the reaction was started by the addition of xanthine. The XO inhibition by various compounds was calculated by the reduction of uric acid production in the first 2 min. Allopurinol and topiroxostat were used as positive controls. All tests were performed in triplicate. Compounds presenting inhibitory effects over 60% at a concentration of 33 μM were further tested at a wide range of concentrations to calculate their IC_{50} values using SPSS 25.0 (SPSS Inc., Chicago, IL, USA) software.

4.3. Molecular docking

Molecular modeling studies were performed with MOE software [46]. The co-crystal structure of bovine XO in complex with topiroxostat (PDB code 1V97) [50] was downloaded from RCSB Protein Data Bank (http://www.rcsb.org/), which was optimized by a series of procedures of Structure Preparation. Protonate 3D and Structure Refine (RMSD gradient = 0.1 kcal/mol, AMBER99 force field) to provide a docking receptor [51]. The ligands were generated by Builder protocol in MOE. The docking procedure was adopted the standard protocol implemented in MOE and all parameters were maintained as the defaults.

4.4. Molecular dynamics simulations

MD simulations studies were performed using GROMACS 5.0 package [52,53]. The CHARMM36 force field was adopted for the simulations [54]. Ligand topology files were generated using CHARMM General Force Field [55]. Corresponding counterions were added to neutralize the solvated TIP3P water model present in the dodecahedron box. The energy was minimized using the steepest descent algorithm. The particle mesh Ewald (PME) method was employed for energy calculation, electrostatic, and Van der Waals interactions. The systems were equilibrated in the NVT ensemble for 20,000 steps followed by equilibration in the NPT ensemble for an additional 20,000 steps. Finally, 20 ns MD simulations were performed at 300 K under periodic boundary conditions with a 2.0 fs time step [56,57].

4.5. Hypouricemic effect in vivo

Twenty-four six-week-old Sprague-Dawley rats, half male and half female, weighing 180–220 g, were provided by Beijing Huafukang Biotechnology Co., Ltd (Beijing, China). The production license number of experimental animals was SCXK 2019-0008. Experimental animals were raised in the SPF Animal Experiment Center of the Laboratory

Animal Department of China Medical University (experimental animal license number: SYXK 2018-0008). The maintenance and treatment of animals complied with the protocol approved by the Animal Experiment Ethics Review Committee of China Medical University. This study was approved by the Laboratory Animal Welfare Ethics Committee of China Medical University (IACUC: NO CMU2020116).

The rats had free access to food and water and kept a 12-hour light-dark cycle in a room with controlled temperature and humidity for one week. After that, the rats were randomly divided into 4 groups of six each as follows: blank group, model group, test (**3i**) group and positive control (topiroxostat) group, and then fasted and free drinking water for 12 h. Subsequently, rats in the blank group were intraperitoneally injected with 2 mL of normal saline (Shandong Kelun Pharmaceutical Co., Ltd, Binzhou, China), and the other groups were intraperitoneally injected with 300 mg/kg of potassium oxonate (Shanghai Yien Chemical Technology Co., Ltd., Shanghai, China) dissolved in 2 mL normal saline to induce a rat model of acute hyperuric acid. One hour after intraperitoneal injection of rats, the blank group and the model group were given 0.5% CMC-Na solution, 2 mL/rat; the positive control group was given topiroxostat (10 mg/kg), and the test group received compound **3i** (12.8 mg/kg), in which both topiroxostat and **3i** were prepared with 2 mL 0.5% CMC-Na solution into a uniform and stable suspension [58,59]. After administration 0.5 h, 1 h, 2 h, 3 h, 4 h, 6 h, 8 h, 700 uL of blood was collected through the orbital vein each time. The collected blood samples were clotted at room temperature for 1 h, and then centrifuged at 3000 g for 10 min at 4 °C. According to the manufacturer's instructions, a uric acid determination kit (Nanjing Jiancheng Institute of Biological Engineering, Nanjing, China) was used to determine serum uric acid levels by UV spectrophotometer (TU-1901) at 690 nm. Statistical analysis was analyzed with Student's *t*-test to determine the significance level. The data are expressed as mean ± standard deviation. The figures were obtained with the GraphPad Prism 7.0 statistical system.

4.6. MTT assay

All healthy cell lines were obtained from the Shanghai Cell Resource Bank. Cultured cells using the culture guidelines provided by the supplier and performed relevant mycoplasma tests once a month.

The cultured cells were collected in the logarithmic growth phase, digested with 0.25% trypsin, and diluted into a single cell suspension with phosphate-buffered saline (PBS). Then 100 μL of each cell type (4×10^4 cells/mL) was seeded into 96-well plate and incubated for 24 h. Different concentrations of compounds were added into the 96-well plates. Respective concentrations of DMSO were used as control. Then these plates were incubated for 24 h, and 20 μL MTT solution (5 mg/mL) (Wuhan Bost Biotechnology Co., Ltd., China) was added and cultured for 4 h. The nutrient solution was discarded slowly and 100 μL of DMSO was added to each well. The optical density (OD) of each well was detected at 490 nm using a microplate reader. The cell viability was expressed as the cytotoxicity of the test compound, and each determination was performed in triplicate. Data were expressed as mean ± SD (n = 3).

4.7. ADME/T properties prediction

For the *in silico* prediction, the Pre-ADMET server application was used [60]. The Pre-ADMET approach is based on different classes of molecular parameters that are considered for generating quantitative structure properties.

Declaration of Competing Interest

The authors declare that they have no known competing financial interests or personal relationships that could have appeared to influence the work reported in this paper.

Acknowledgments

This work was supported by the National Natural Science Foundation of China (Grant No. 81803355) and Young Talents Program of China Medical University.

Appendix A. Supplementary material

Supplementary data to this article can be found online at https://doi.org/10.1016/j.bioorg.2021.105181.

References

[1] F. Perez-Ruiz, N. Dalbeth, T. Bardin, A review of uric acid, crystal deposition disease, and gout, Adv. Ther. 32 (2015) 31–41.
[2] P. Richette, M. Doherty, E. Pascual, V. Barskova, F. Becce, J. Castañeda-Sanabria, M. Coyfish, S. Guillo, T.L. Jansen, H. Janssens, F. Lioté, C. Mallen, G. Nuki, F. Perez-Ruiz, J. Pimentao, L. Punzi, T. Pywell, A. So, A.K. Tausche, T. Uhlig, J. Zavada, W. Zhang, F. Tubach, T. Bardin, updated EULAR evidence-based recommendations for the management of gout, Ann. Rheum. Dis. 76 (2017) (2016) 29–42.
[3] C. Diaz-Torné, N. Perez-Herrero, F. Perez-Ruiz, New medications in development for the treatment of hyperuricemia of gout, Curr. Opin. Rheumatol. 27 (2015) 164–169.
[4] A.M. Abeles, M.H. Pillinger, Gout and cardiovascular disease: crystallized confusion, Curr. Opin. Rheumatol. 31 (2019) 118–124.
[5] T.T. Braga, O. Foresto-Neto, N. Camara, The role of uric acid in inflammasome-mediated kidney injury, Curr. Opin. Nephrol. Hypertens. 29 (2020) 423–431.
[6] Y. Xia, Q. Wu, H. Wang, S. Zhang, Y. Jiang, T. Gong, X. Xu, Q. Chang, K. Niu, Y. Zhao, Global, regional and national burden of gout, 1990–2017: a systematic analysis of the global burden of disease study, Rheumatology (Oxford) 59 (2020) 1529–1538.
[7] R. Kumar, G. Joshi, H. Kler, S. Kalra, M. Kaur, R. Arya, Toward an understanding of structural insights of xanthine and aldehyde oxidases: An overview of their Inhibitors and role in various diseases, Med. Res. Rev. 38 (2018) 1073–1125.
[8] Z. Smelcerovic, A. Veljkovic, G. Kocic, D. Yancheva, Z. Petronijevic, M. Anderluh, A. Smelcerovic, Xanthine oxidase inhibitory properties and anti-inflammatory activity of 2-amino-5-alkylidene-thiazol-4-ones, Chem. Biol. Interact. 229 (2015) 73–81.
[9] S. Li, T. Zhang, Q. Wu, K.M. Olounfeh, Y. Zhang, F. Meng, Synthesis and biological evaluation of 5-benzyl-3-pyridyl-1H-1,2,4-triazole derivatives as xanthine oxidase inhibitors, Med. Chem. 16 (2020) 119–127.
[10] M. Negi, M.J. Mulla, C.S. Han, V.M. Abrahams, Allopurinol inhibits excess glucose-induced trophoblast IL-1 beta and ROS production, Reproduction 159 (2020) 73–80.
[11] B. Zhang, X. Dai, Z. Bao, Q. Mao, Y. Duan, Y. Yang, S. Wang, Targeting the subpocket in xanthine oxidase: Design, synthesis, and biological evaluation of 2-[4-alkoxy-3-(1H-tetrazol-1-yl) phenyl]-6-oxo-1,6-dihydropyrimidine-5-carboxylic acid derivatives, Eur. J. Med. Chem. 181 (2019), 111559.
[12] S.V. Badve, E.M. Pascoe, A. Tiku, N. Boudville, F.G. Brown, A. Cass, P. Clarke, N. Dalbeth, R.O. Day, J.R. de Zoysa, B. Douglas, R. Faull, D.C. Harris, C.M. Hawley, G. Jones, J. Kanellis, S.C. Palmer, V. Perkovic, G.K. Rangan, D. Reidlinger, L. Robison, R.J. Walker, G. Walters, D.W. Johnson, Effects of allopurinol on the progression of chronic kidney disease, N. Engl. J. Med. 382 (2020) 2504–2513.
[13] R. Seth, A.S. Kydd, R. Buchbinder, C. Bombardier, C.J. Edwards, Allopurinol for chronic gout, Cochrane Database Syst. Rev. D6077 (2014).
[14] H.J. Tang, W. Li, M. Zhou, L.Y. Peng, J.X. Wang, J.H. Li, J. Chen, Synthesis and biological evaluation of novel xanthine oxidase inhibitors bearing a 2-arylbenzofuran scaffold, Eur. J. Med. Chem. 151 (2018) 849–860.
[15] M. Kaur, A. Kaur, S. Mankotia, H. Singh, A. Singh, J.V. Singh, M.K. Gupta, S. Sharma, K. Nepali, P.M.S. Bedi, Synthesis, screening and docking of fused pyrano [3,2-d]pyrimidine derivatives as xanthine oxidase inhibitor, Eur. J. Med. Chem. 131 (2017) 14–28.
[16] M.D. Santi, Z.M. Paulino, B. Vera, C. Bouzidi, V. Dumontet, A. Abin-Carriquiry, R. Grougnet, M.G. Ortega, Xanthine oxidase inhibitory activity of natural and hemisynthetic flavonoids from Gardenia oudiepe (Rubiaceae) *in vitro* and molecular docking studies, Eur. J. Med. Chem. 143 (2018) 577–582.
[17] J.H. Kim, C.H. Jin, Xanthine oxidase inhibitory activity of isoflavonoids from Apios americana, Comput. Biol. Chem. 83 (2019), 107137.
[18] S. Chen, T. Zhang, J. Wang, F. Wang, H. Niu, C. Wu, S. Wang, Synthesis and evaluation of 1-hydroxy/methoxy-4-methyl-2-phenyl-1H-imidazole-5-carboxylic acid derivatives as non-purine xanthine oxidase inhibitors, Eur. J. Med. Chem. 103 (2015) 343–353.
[19] I. Fatima, H. Zafar, K.M. Khan, S.M. Saad, S. Javaid, S. Perveen, M.I. Choudhary, Synthesis, molecular docking and xanthine oxidase inhibitory activity of 5-aryl-1H-tetrazoles, Bioorg. Chem. 79 (2018) 201–211.
[20] G. Kaur, J.V. Singh, M.K. Gupta, K. Bhagat, H.K. Gulati, A. Singh, P.M.S. Bedi, H. Singh, S. Sharma, Thiazole-5-carboxylic acid derivatives as potent xanthine oxidase inhibitors: design, synthesis, in vitro evaluation, and molecular modeling studies, Med. Chem. Res. 29 (2020) 83–93.
[21] Q. Mao, X. Dai, G. Xu, Y. Su, B. Zhang, D. Liu, S. Wang, Design, synthesis and biological evaluation of 2-(4-alkoxy-3-cyano)phenyl-6-oxo-1,6-dihydropyrimidine-

5-carboxylic acid derivatives as novel xanthine oxidase inhibitors, Eur. J. Med. Chem. 181 (2019), 111558.
[22] D. Sato, T. Kisen, M. Kumagai, K. Ohta, Synthesis, structure-activity relationships, and mechanistic studies of 5-arylazo-tropolone derivatives as novel xanthine oxidase (XO) inhibitors, Bioorg. Med. Chem. 26 (2018) 536–542.
[23] W. Choi, V. Villegas, H. Istre, B. Heppler, N. Gonzalez, N. Brusman, L. Snider, E. Hogle, J. Tucker, A. Onate, S. Onate, L. Ma, S. Paula, Synthesis and characterization of CAPE derivatives as xanthine oxidase inhibitors with radical scavenging properties, Bioorg. Chem. 86 (2019) 686–695.
[24] S. Burmaoglu, S. Ozcan, S. Balcioglu, M. Gencel, S. Noma, S. Essiz, B. Ates, O. Algul, Synthesis, biological evaluation and molecular docking studies of bis-chalcone derivatives as xanthine oxidase inhibitors and anticancer agents, Bioorg. Chem. 91 (2019), 103149.
[25] Z. Xie, X. Luo, Z. Zou, X. Zhang, F. Huang, R. Li, S. Liao, Y. Liu, Synthesis and evaluation of hydroxychalcones as multifunctional non-purine xanthine oxidase inhibitors for the treatment of hyperuricemia, Bioorg. Med. Chem. Lett. 27 (2017) 3602–3606.
[26] T. Hosoya, T. Ishikawa, Y. Ogawa, R. Sakamoto, T. Ohashi, Multicenter, Open-label study of long-term topiroxostat (FYX-051) administration in Japanese hyperuricemic patients with or without gout, Clin. Drug Investig. 38 (2018) 1135–1143.
[27] T.J. Zhang, S.Y. Li, L. Wang, Q. Sun, Q.X. Wu, Y. Zhang, F.H. Meng, Design, synthesis and biological evaluation of N-(4-alkoxy-3-cyanophenyl) isonicotinamide/nicotinamide derivatives as novel xanthine oxidase inhibitors, Eur. J. Med. Chem. 141 (2017) 362–372.
[28] T.J. Zhang, S.Y. Li, W.Y. Yuan, Q.X. Wu, L. Wang, S. Yang, Q. Sun, F.H. Meng, Discovery and biological evaluation of some (1H–1,2,3-triazol-4-yl) methoxybenzaldehyde derivatives containing an anthraquinone moiety as potent xanthine oxidase inhibitors, Bioorg. Med. Chem. Lett. 27 (2017) 729–732.
[29] T.J. Zhang, S.Y. Li, W.Y. Yuan, Y. Zhang, F.H. Meng, Design, synthesis, and molecular docking studies of N-(9,10-anthraquinone-2-carbonyl)amino acid derivatives as xanthine oxidase inhibitors, Chem. Biol. Drug Des. 91 (2018) 893–901.
[30] T.J. Zhang, S.Y. Li, Y. Zhang, Q.X. Wu, F.H. Meng, Design, synthesis, and biological evaluation of 5-(4-(pyridin-4-yl)-1H-1,2,3-triazol-1-yl)benzonitrile derivatives as xanthine oxidase inhibitors, Chem. Biol. Drug Des. 91 (2018) 526–533.
[31] T.J. Zhang, Q.X. Wu, S.Y. Li, L. Wang, Q. Sun, Y. Zhang, F.H. Meng, H. Gao, Synthesis and evaluation of 1-phenyl-1H-1,2,3-triazole-4-carboxylic acid derivatives as xanthine oxidase inhibitors, Bioorg. Med. Chem. Lett. 27 (2017) 3812–3816.
[32] T.J. Zhang, Y. Zhang, S. Tu, Y.H. Wu, Z.H. Zhang, F.H. Meng, Design, synthesis and biological evaluation of N-(3-(1H-tetrazol-1-yl)phenyl)isonicotinamide derivatives as novel xanthine oxidase inhibitors, Eur. J. Med. Chem. 183 (2019), 111717.
[33] T. Zhang, Y. Lv, Y. Lei, D. Liu, Y. Feng, J. Zhao, S. Chen, F. Meng, S. Wang, Design, synthesis and biological evaluation of 1-hydroxy-2-phenyl-4-pyridyl-1H-imidazole derivatives as xanthine oxidase inhibitors, Eur. J. Med. Chem. 146 (2018) 668–677.
[34] P.F. Rosales, G.S. Bordin, A.E. Gower, S. Moura, Indole alkaloids: 2012 until now, highlighting the new chemical structures and biological activities, Fitoterapia 143 (2020), 104558.
[35] V. Garg, R.K. Maurya, P.V. Thanikachalam, G. Bansal, V. Monga, An insight into the medicinal perspective of synthetic analogs of indole: A review, Eur. J. Med. Chem. 180 (2019) 562–612.
[36] A. Kumari, R.K. Singh, Medicinal chemistry of indole derivatives: Current to future therapeutic prospectives, Bioorg. Chem. 89 (2019), 103021.
[37] J.U. Song, J.W. Jang, T.H. Kim, H. Park, W.S. Park, S.H. Jung, G.T. Kim, Structure-based design and biological evaluation of novel 2-(indol-2-yl) thiazole derivatives as xanthine oxidase inhibitors, Bioorg. Med. Chem. Lett. 26 (2016) 950–954.
[38] J.U. Song, S.P. Choi, T.H. Kim, C.K. Jung, J.Y. Lee, S.H. Jung, G.T. Kim, Design and synthesis of novel 2-(indol-5-yl)thiazole derivatives as xanthine oxidase inhibitors, Bioorg. Med. Chem. Lett. 25 (2015) 1254–1258.
[39] C. Enroth, B.T. Eger, K. Okamoto, T. Nishino, T. Nishino, E.F. Pai, Crystal structures of bovine milk xanthine dehydrogenase and xanthine oxidase: structure-based mechanism of conversion, Proc. Natl. Acad. Sci. U. S. A. 97 (2000) 10723–10728.
[40] K. Chen, Y.L. Zhang, J. Fan, X. Ma, Y.J. Qin, H.L. Zhu, Novel nicotinoyl pyrazoline derivates bearing N-methyl indole moiety as antitumor agents: Design, synthesis and evaluation, Eur. J. Med. Chem. 156 (2018) 722–737.
[41] D. Kumar, M.K. Narayanam, K.H. Chang, K. Shah, Synthesis of novel indolyl-1,2,4-triazoles as potent and selective anticancer agents, Chem. Biol. Drug Des. 77 (2011) 182–188.
[42] Y. Lu, J. Chen, J. Wang, C.M. Li, S. Ahn, C.M. Barrett, J.T. Dalton, W. Li, D. D. Miller, Design, synthesis, and biological evaluation of stable colchicine binding site tubulin inhibitors as potential anticancer agents, J. Med. Chem. 57 (2014) 7355–7366.
[43] L.C. Miller, C.T. O'Loughlin, Z. Zhang, A. Siryaporn, J.E. Silpe, B.L. Bassler, M. F. Semmelhack, Development of potent inhibitors of pyocyanin production in Pseudomonas aeruginosa, J. Med. Chem. 58 (2015) 1298–1306.
[44] Q. Xia, X. Bao, C. Sun, D. Wu, X. Rong, Z. Liu, Y. Gu, J. Zhou, G. Liang, Design, synthesis and biological evaluation of novel 2-sulfonylindoles as potential anti-inflammatory therapeutic agents for treatment of acute lung injury, Eur. J. Med. Chem. 160 (2018) 120–132.
[45] M. Hylsová, B. Carbain, J. Fanfrlík, L. Musilová, S. Haldar, C. Köprülüoğlu, H. Ajani, P.S. Brahmkshatriya, R. Jorda, V. Kryštof, P. Hobza, A. Echalier, K. Paruch, M. Lepšík, Explicit treatment of active-site waters enhances quantum mechanical/implicit solvent scoring: Inhibition of CDK2 by new pyrazolo[1,5-a] pyrimidines, Eur. J. Med. Chem. 126 (2017) 1118–1128.
[46] S. Vilar, G. Cozza, S. Moro, Medicinal chemistry and the molecular operating environment (MOE): application of QSAR and molecular docking to drug discovery, Curr. Top. Med. Chem. 8 (2008) 1555–1572.
[47] GROMACS: High performance molecular simulations through multi-level parallelism from laptops to supercomputers, Softwarex 1-2 (2015) 19-25.
[48] M. Rashid, Design, synthesis and ADMET prediction of bis-benzimidazole as anticancer agent, Bioorg. Chem. 96 (2020), 103576.
[49] K. Matsumoto, K. Okamoto, N. Ashizawa, T. Nishino, FYX-051: a novel and potent hybrid-type inhibitor of xanthine oxidoreductase, J. Pharmacol. Exp. Ther. 336 (2011) 95–103.
[50] K. Okamoto, K. Matsumoto, R. Hille, B.T. Eger, E.F. Pai, T. Nishino, The crystal structure of xanthine oxidoreductase during catalysis: implications for reaction mechanism and enzyme inhibition, Proc. Natl. Acad. Sci. U. S. A. 101 (2004) 7931–7936.
[51] S.H. Abbas, G. Abuo-Rahma, M. Abdel-Aziz, O.M. Aly, E.A. Beshr, A.M. Gamal-Eldeen, Synthesis, cytotoxic activity, and tubulin polymerization inhibitory activity of new pyrrol-2(3H)-ones and pyridazin-3(2H)-ones, Bioorg. Chem. 66 (2016) 46–62.
[52] P. Szilárd, M.J. Abraham, C. Kutzner, B. Hess, E. Lindahl, Tackling exascale software challenges in molecular dynamics simulations with GROMACS In S. Markidis & E. Laure (Eds.), Solving Software Challenges for Exascale, 8759 (2015) 3-27.
[53] S. Pronk, S. Páll, R. Schulz, P. Larsson, E. Lindahl, GROMACS 4.5: A high-throughput and highly parallel open source molecular simulation toolkit, Bioinformatics 29 (2013) 845-854.
[54] J. Huang, A.J. MacKerell, CHARMM36 all-atom additive protein force field: validation based on comparison to NMR data, J. Comput. Chem. 34 (2013) 2135–2145.
[55] K. Vanommeslaeghe, E. Hatcher, C. Acharya, S. Kundu, S. Zhong, J. Shim, E. Darian, O. Guvench, P. Lopes, I. Vorobyov, A.J. Mackerell, CHARMM general force field: A force field for drug-like molecules compatible with the CHARMM all-atom additive biological force fields, J. Comput. Chem. 31 (2010) 671–690.
[56] R. Dolezal, O. Soukup, D. Malinak, R. Savedra, J. Marek, M. Dolezalova, M. Pasdiorova, S. Salajkova, J. Korabecny, J. Honegr, T.C. Ramalho, K. Kuca, Towards understanding the mechanism of action of antibacterial N-alkyl-3-hydroxypyridinium salts: Biological activities, molecular modeling and QSAR studies, Eur. J. Med. Chem. 121 (2016) 699–711.
[57] M.C. Childers, V. Daggett, Validating molecular dynamics simulations against sxperimental observables in light of underlying conformational ensembles, J. Phys. Chem. B 122 (2018) 6673–6689.
[58] Y.C. Zeng, S. Li, C. Liu, T. Gong, X. Sun, Y. Fu, Z.R. Zhang, Soluplus micelles for improving the oral bioavailability of scopoletin and their hypouricemic effect *in vivo*, Acta Pharmacol. Sin. 38 (2017) 424–433.
[59] J. Gao, Z. Zhang, B. Zhang, Q. Mao, X. Dai, Q. Zou, Y. Lei, Y. Feng, S. Wang, Novel 3-[4-alkoxy-3-(1H-tetrazol-1-yl) phenyl]-1,2,4-oxadiazol-5(4H)-ones as promising xanthine oxidase inhibitors: Design, synthesis and biological evaluation, Bioorg. Chem. 95 (2020), 103564.
[60] M.T.H. Khan, I. Sylte, Multivariate linear regression models based on ADME descriptors and predictions of ADMET profile for structurally diverse thermolysin inhibitors, Lett. Drug Des. Discov. 6 (2009) 428–436.